NIST Technical Note
NIST TN 2373

Thermophysical Properties of 2,3,3,4,4,4-Hexafluoro-1-butene [R-1336yf]: Measurements and an Equation of State

Tara J. Fortin
Marcia L. Huber
Andrei F. Kazakov
Stephanie L. Outcalt
Aaron J. Rowane

This publication is available free of charge from:
https://doi.org/10.6028/NIST.TN.2373

NIST NATIONAL INSTITUTE OF STANDARDS AND TECHNOLOGY
U.S. DEPARTMENT OF COMMERCE

NIST Technical Note
NIST TN 2373

Thermophysical Properties of 2,3,3,4,4,4-Hexafluoro-1-butene [R-1336yf]: Measurements and an Equation of State

Tara J. Fortin
Marcia L. Huber
Andrei F. Kazakov
Stephanie L. Outcalt*
Aaron J. Rowane
Applied Chemicals and Materials Division
Material Measurement Laboratory

**Former NIST employee; all work for this publication was done while at NIST.*

This publication is available free of charge from:
https://doi.org/10.6028/NIST.TN.2373

August 2026

U.S. Department of Commerce
Howard Lutnick, Secretary

National Institute of Standards and Technology
Arvind Raman, Under Secretary of Commerce for Standards and Technology and NIST Director

NIST TN 2373
August 2026

Certain equipment, instruments, software, or materials, commercial or non-commercial, are identified in this paper in order to specify the experimental procedure adequately. Such identification does not imply recommendation or endorsement of any product or service by NIST, nor does it imply that the materials or equipment identified are necessarily the best available for the purpose.

NIST Technical Series Policies
Copyright, Use, and Licensing Statements
NIST Technical Series Publication Identifier Syntax

Publication History
Approved by the NIST Editorial Review Board on 2026-04-14

How to Cite this NIST Technical Series Publication
Fortin TJ, Huber ML, Kazakov AF, Outcalt SL, Rowane AJ.(2026) Thermophysical Properties of 2,3,3,4,4,4-Hexafluoro-1-butene [R-1336yf]: Measurements and an Equation of State. (National Institute of Standards and Technology, Gaithersburg, MD), NIST Technical Note (TN) NIST TN 2373. https://doi.org/10.6028/NIST.TN.2373

Author ORCID iDs
Tara J. Fortin: 0000-0001-6150-8930
Marcia L. Huber: 0000-0002-7976-741X
Andrei F. Kazakov: 0009-0008-6964-3086
Stephanie L. Outcalt: 0000-0001-8143-7316
Aaron J. Rowane: 0000-0001-7605-0774

Contact Information
tara.fortin@nist.gov

Abstract

We report thermodynamic property measurements for the refrigerant R-1336yf (2,3,3,4,4,4-hexafluoro-1-butene), which is being considered as a replacement for existing refrigerants. Density (ρ) data were measured in the compressed liquid phase at temperatures from 270 K to 410 K and pressures from 0.5 MPa to 30 MPa. Vapor pressure (p_{sat}) data were measured from 265 K to 360 K. Speed of sound (w) data were measured in the liquid phase from 230 K to 373 K and pressures up to 10 MPa. Relative combined, expanded (95% confidence level) uncertainties ranged from 0.04 % to 0.18 % for density, from 0.31 % to 0.59 % for vapor pressure, and from 0.27 % to 0.97 % for speed of sound. These reported uncertainties are larger than our typical pure fluid results due to the presence of significant sample impurities. These data have been used to develop a new equation of state explicit in the Helmholtz energy. The equation of state represents the experimental data with an average absolute relative deviation (AARD) of 0.16 % for density, 1.15 % for vapor pressure, and 0.27 % for speed of sound.

Keywords

Density; equation of state; hydrofluoroolefin; refrigerants; speed of sound; vapor pressure.

Table of Contents

List of Tables

List of Figures

Acknowledgments

The authors thank our NIST colleagues Dr. Jason Widegren, Dr. Chris Suiter, Dr. Nathan Bryant, Dr. Samantha Miller, and Dr. Tara Lovestead for providing compositional analysis of R-1336mzz(Z) and R-1336yf, and Dr. Eric Lemmon for guidance on the fitting methodology and EOS development. Additionally, the authors thank Dr. Ryo Akasaka for helpful discussions regarding the EOS development. This work was supported by the Office of Naval Research under Agreement MIPR N0001422IP00032 with Dr. Mark Spector serving as program manager.

1. Introduction

In response to regulatory changes, significant research effort has been focused on the search for the next generation of refrigerants to replace many of the second and third generation refrigerants originally developed to replace chlorofluorocarbons (CFCs). Extensive analyses of potential replacements have demonstrated that only a limited group of fluids exhibit the properties required for low- and medium-temperature refrigeration applications [1-4]. Of these, hydrofluoroolefins (HFOs) are considered one of the most promising groups of compounds.

One such HFO of interest is R-1336yf (2,3,3,4,4,4-hexafluoro-1-butene). The development of an accurate model to effectively analyze the performance of a new refrigerant such as R-1336yf requires reliable thermophysical property data. Unfortunately, only two experimental vapor pressure values [5] and a limited set of simulation data [6] are available in the literature for this fluid, making the development of a model impossible. In this work, we report thermophysical property measurement results for R-1336yf. Specifically, we report the results for liquid density, vapor pressure, and liquid speed of sound measurements covering the overall temperature range of approximately 230 K to 410 K and pressures up to 30 MPa. These measurements, along with computational chemistry calculations for the ideal-gas heat capacity, were then utilized in the development of a new Helmholtz-energy-explicit equation of state, which is also discussed here.

2. Experimental Section

2.1 Sample Materials

Refrigerants measured in this work are listed in Table 1, along with the corresponding chemical formula, CAS number, supplier, and sample purity. Molecular representations constructed using Avogadro [7] are shown in Fig. 1. R-1336mzz(Z) was used as the calibration fluid for the density measurements reported in this work; it had a manufacturer's stated purity of 99.99 mole %, which was confirmed by gas-chromatography/quadrupole time-of-flight mass spectroscopy (GC/QToF-MS) measurements performed at NIST. The purity of the primary measurement sample, R-1336yf, was determined entirely via measurements performed at NIST. Specifically, a combination of Coulometric Karl-Fischer Titration, GC/QToF-MS, and nuclear magnetic resonance (NMR) spectroscopy measurements were used to determine a purity. Although every effort was made to secure the highest-purity sample available, extensive compositional analysis indicated a purity of 97.69 mol % for R-1336yf. Water was the primary impurity identified (1.09 mol %); other impurities present in quantifiable amounts were acetaldehyde (0.672 mol %), 1,1,1,2,2,3,3,3-heptafluorobutane (0.404 mol %), methyl acetate (0.092 mol %), pentaerythritol tetrapentanoate (0.026 mol %), and 3,3,3-trifluoropropene (0.023 mol %).

Table 1. Chemical information.

Refrigerant	Chemical Name	Chemical Formula	CAS	Supplier[1]	Purity[a]
R-1336mzz(Z)	*cis*-1,1,1,4,4,4-hexafluoro-2-butene	$C_4H_2F_6$	692-49-9	Chemours	0.9999
R-1336yf	2,3,3,4,4,4-hexafluoro-1-butene	$C_4H_2F_6$	374-39-0	SynQuest Laboratories	0.9769

[a]Sample purity in mole fraction.

Prior to measurements, each refrigerant was transferred from its manufacturer's container to a clean stainless-steel sample cylinder. The samples were then degassed to remove volatile impurities by repeat freeze-pump-thaw cycles that involved freezing the sample in liquid nitrogen, evacuating the vapor space over the frozen sample, and then thawing the sample; the cycles were repeated until a negligible increase in pressure is observed during the evacuation step.

[1] In order to describe materials and experimental procedures adequately, it is occasionally necessary to identify commercial products by manufacturers' names or labels. In no instance does such identification imply endorsement by the National Institute of Standards and Technology, nor does it imply that the particular product or equipment is necessarily the best available for the purpose.

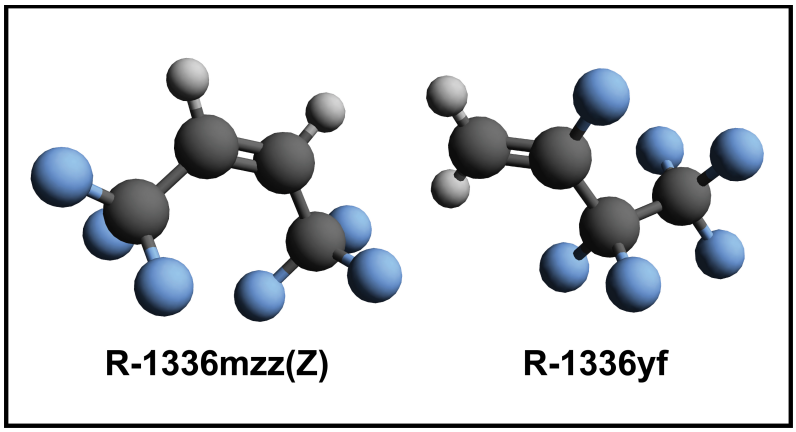

Fig. 1. Molecular representations of refrigerants measured in this work. R-1336mzz(Z) was used as a calibration fluid for the density measurements. Carbon atoms are black, hydrogen atoms are gray, and fluorine atoms are blue. Diagrams were constructed using Avogadro [7].

2.2 Experimental Apparatus

The experimental apparatuses employed in this work have been described in detail in previous publications [8-11]; only brief descriptions are provided here.

2.2.1 Vibrating Tube Densimeter

A vibrating tube densimeter (VTD) was used to measure the compressed liquid densities reported in this work. At the heart of the apparatus is a commercial VTD made of Hastelloy C-276. The commercial instrument has been modified to improve temperature control, as well as the accuracy of both temperature and pressure measurements, and to allow for automated operation of the instrument [8]. As designed, the instrument operates over the temperature range from 270 K to 470 K and pressures up to 70 MPa. Temperature is measured with a standard platinum resistance thermometer (SPRT) and is controlled with thin-film heaters; a circulating bath is also used for temperatures $\leq$ 300 K. Upon reaching thermal equilibrium, the instrument temperature remains stable to within $\pm$ 5 mK; the combined standard uncertainty in temperature is $\leq$ 15 mK. Pressure is measured with an oscillating quartz crystal pressure transducer and is controlled with a programmable syringe pump; the combined standard uncertainty in pressure is $\leq$ 5 kPa.

The fundamental measurement principle is that the period of oscillation (τ) of a resonating hollow U-shaped tube can be related to the density (ρ) of the fluid that fills it. This can be expressed as

$$\rho = A\tau^2 - B \tag{1}$$

where A and B are apparatus-specific parameters that vary with both temperature and pressure and must be determined by calibration both with the tube under vacuum (i.e., τ_0) and with the tube filled with a calibration fluid [12]. In this work, we used R-1336mzz(Z) as the

calibration fluid and the physically-based model proposed by May et al. [13] as the calibration equation. The results of our calibration with R-1336mzz(Z) are shown in Fig. 2, plotted as percent deviation from the equation of state [14] included in REFPROP (version 10.0) [15] vs temperature. Here, the average absolute relative deviation (AARD) and the maximum relative deviation (MRD) were 0.01 % and 0.03 %, respectively. AARD was calculated as

$$\mathrm{AARD} = \frac{1}{n}\sum_{i=1}^{n}|\mathrm{PCT}|_i, \tag{2}$$

and MRD as

$$\mathrm{MRD} = \max(\mathrm{PCT}), \tag{3}$$

with

$$\mathrm{PCT} = 100 \cdot \left(\frac{X_{\mathrm{exp}} - X_{\mathrm{calc}}}{X_{\mathrm{exp}}}\right). \tag{4}$$

Here, X_{exp} is the experimental value for some thermodynamic property X (e.g., ρ), X_{calc} is the corresponding calculated value, and n is the total number of data points.

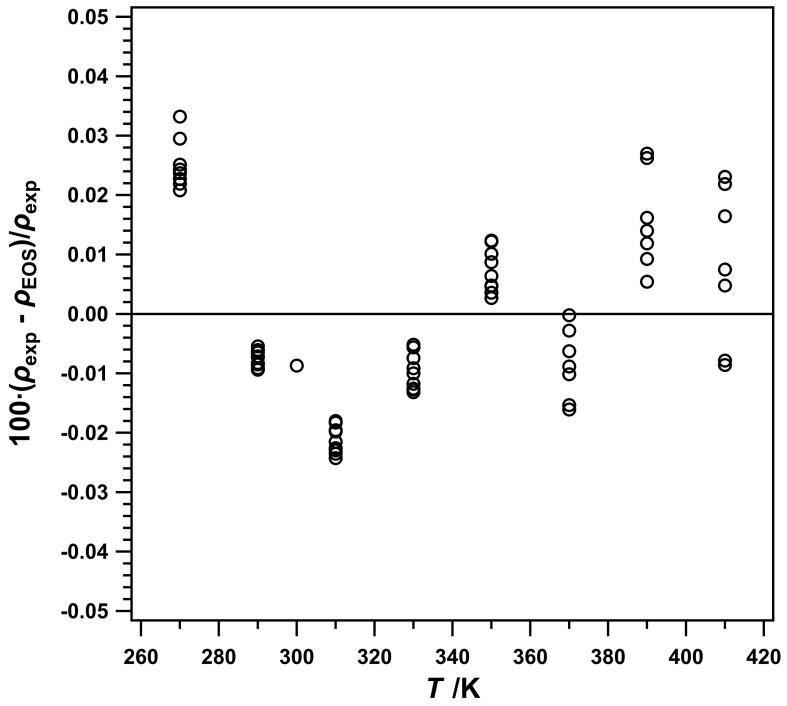

Fig. 2. Relative deviations of measured density data for R-1336mzz(Z) from values calculated with the EOS [14] included in REFPROP (Version 10) [15], plotted as a function of temperature.

2.2.2 Vapor-Liquid Equilibria Apparatus

A vapor-liquid equilibria (VLE) apparatus was used to measure the vapor pressures reported in this work. The equilibrium cell is a stainless-steel cylinder with sapphire windows on both ends so that the liquid level inside is visible. The cell is housed within a thermostated aluminum block and temperature is measured with an SPRT. Vapor pressure is measured with one of two oscillating-quartz-crystal pressure transducers. The first transducer has a maximum pressure of 0.7 MPa, while the maximum pressure for the second transducer is 7 MPa. Overall, the instrument is operable over the temperature range from 265 K to 360 K and pressures up to 7 MPa. Further details on the VLE apparatus can be found in Outcalt and Rowane [9].

2.2.3 Dual-Path Pulse-Echo Apparatus

A dual-path pulse-echo apparatus was used to measure the speeds of sound reported in this work. At the core of the instrument, submerged in the fluid of interest, is an x-cut quartz crystal with a resonant frequency of 8 MHz. The crystal is sandwiched between two ceramic spacers with lengths of 12 mm and 30 mm, which define the short and long paths of the instrument, respectively. An arbitrary function generator is used to excite the quartz-crystal transducer with a 10-cycle sinusoidal tone-burst creating ultrasonic pulses emitted from both faces of the crystal. These ultrasonic pulses traverse the short and long paths of the instrument until they are reflected off planar surfaces at the end of each spacer and returned to the crystal, which also serves as a signal detector. The echoes are recorded using a digital storage oscilloscope and are used to determine the time difference between the arrival of the short and long path echoes. The governing equation for the dual-path pulse-echo instrument used to obtain the speed of sound is

$$w = \frac{2\left(L_{\mathrm{long}} - L_{\mathrm{short}}\right)}{\left(\Delta t + \delta t_{\mathrm{d}}\right)}, \tag{5}$$

where w is the speed of sound, L_{long} and L_{short} are long and short path lengths defined by the ceramic spacers, Δt is the time difference between the short and long path echo arrivals, and δt_{d} is a diffraction correction due to a difference in the phase advance of the actual sound wave versus that of a perfect plane wave [16]. The difference between L_{long} and L_{short} was determined by calibration with propane using the equation of state of Lemmon et al. [17]. The procedure used to determine both Δt and δt_{d} for this instrument is described by McLinden and Perkins [10] and Rowane and Rasmussen [18].

2.3 Measurement Procedures

2.3.1 Vibrating Tube Densimeter

Prior to starting density measurements, the evacuated syringe pump was filled with degassed sample; the syringe pump was then used to fill the evacuated measurement cell with compressed liquid sample. Measurements of the compressed liquid were made along

isotherms starting at 270 K and increasing to 410 K in 20 K increments. For each isotherm, measurements were made from the highest to the lowest pressure, which in this work ranged from 30 MPa to a low of 0.5 MPa. The minimum pressure for each isotherm was selected to restrict measurements to the compressed fluid region. Once measurements were completed for the full surface, additional measurements were made to check repeatability; in this work, repeat measurements were performed for four isotherms at 270 K, 290 K, 310 K, and 370 K.

2.3.2 Vapor-Liquid Equilibria Apparatus

Prior to starting vapor pressure measurements, the entire system was evacuated, and sample was loaded such that the cell was almost full of liquid with only a small vapor bubble present. Sample vapor pressures were measured from 265 K to 360 K in 5 K increments. As the temperature increased, a distinct vapor phase was maintained by venting a small amount of liquid from the bottom of the cell. Upon completion of the first run, the cell was cooled down, and fresh sample was added to the remaining cell contents to replace volume that had been vented at higher temperatures. Measurements were then made from 265 K to 355 K in 10 K increments to check repeatability.

2.3.3 Dual-Path Pulse-Echo Apparatus

Before loading the sample, the dual-path pulse-echo instrument, manifold, and filling lines were evacuated for 12 hours. The measuring cell was cooled down to 228.15 K prior to heating the sample bottle and then filling the measuring cell and manifold with sample. Measurements were carried out along pseudo-isochores where the temperature was increased in increments ranging from 1 K to 3 K. Immediately following the filling procedure, vapor-phase R-1336yf remained in the system manifold; therefore, the measured pressure corresponded to the saturation pressure at a temperature intermediate between that of the room temperature and the cell. We referred to this phase of the measurements as the “saturation trace” in an earlier publication [11]. Once the cell temperature reached 235 K, the manifold was filled with liquid and any increase in the temperature resulted in an appreciable increase in pressure. In this state, measurements occurred along pseudo-isochores where the only changes in the internal volumes of the instrument were due to thermal expansion and compressibility. The maximum pressure of the pseudo-isochores was limited to 9.8 MPa as a precaution to avoid a potential polymerization reaction. To start a new pseudo-isochore, the temperature was set to 5 K higher than the previous and sample was vented from the system to vary the starting sample density. Pseudo-isochores were measured in this manner up to a maximum temperature of 373 K.

3. Experimental Results

The state points for the densities, vapor pressures, and sound speeds measured in this work are shown in Fig. 3. These data are reported in Tables 2 to 4 and are described in the following sections.

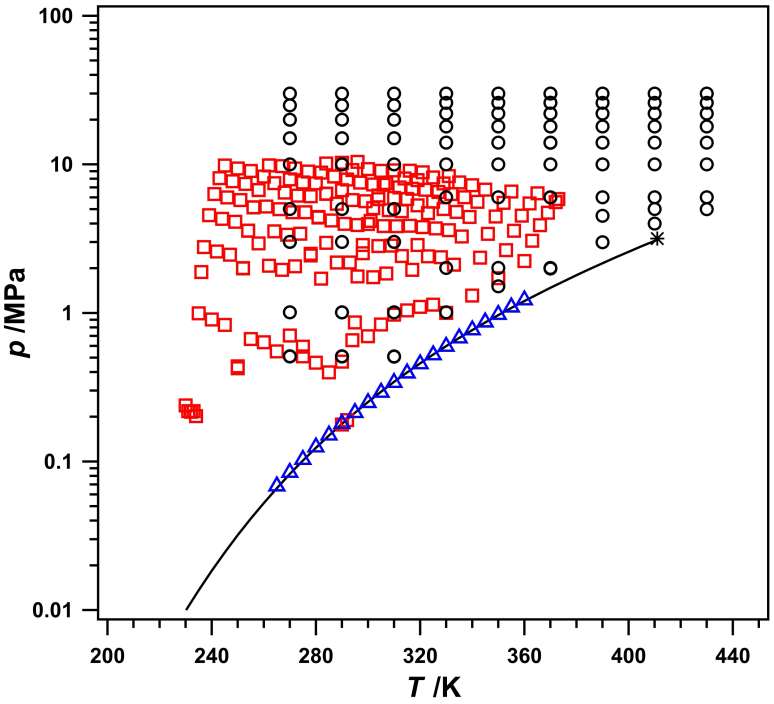

Fig. 3. Pressure-temperature (p-T) state points measured for R-1336yf in this work: density (○), vapor pressure (△), and speed of sound (□). The saturation curve (—) and critical point (✳) shown were calculated using the new EOS developed as part of this work.

3.1 Density

The measured pressure-density-temperature (p-ρ-T) state points for R-1336yf are shown in Fig. 4, plotted as pressure vs density. In this figure, both sets of measurements, referred to as 'Run 1' and 'Run 2', are distinguished by different markers and isotherms are color-coded and labeled. The data shown in Fig. 4 are also presented in Table 2, along with the combined expanded uncertainty in density ($U(\rho)$), which was calculated as

$$U(\rho) = t_{95}(df_\rho) \cdot u(\rho) \tag{6}$$

where $t_{95}(df_\rho)$ is the coverage factor taken from the t-distribution for df_ρ degrees of freedom and a 95 % level of confidence and $u(\rho)$ is the combined standard uncertainty in density. Corresponding $t_{95}(df_\rho)$ values are included in Table 2 for clarity. The determination of df_ρ and $u(\rho)$ are discussed in Sec. 3.4.1. Note that the reported values are averages of 10 replicate measurements at each (T, p) state point. Densities for nominally overlapping state points

between Run 1 and Run 2 agree within 0.10 kg·m^{-3} on average, well within estimated uncertainties.

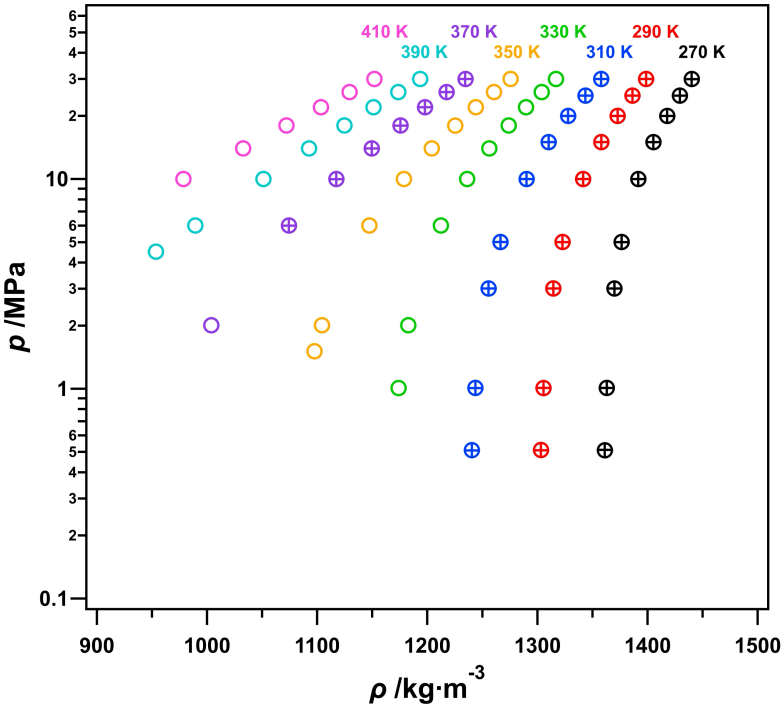

Fig. 4. Measured density data for R-1336yf, plotted as pressure vs density. Here, ○ represent data for Run 1 and + represent data for Run 2. Isotherms are distinguished by color, as labeled.

Table 2. Measured Temperature (T), Pressure (p), and Density (ρ) Data for R-1336yf.[a]

T[b] /K	p[c] /MPa	ρ /kg·m^{-3}	$t_{95}(df_\rho)$[d]	$U(\rho)$[e] /kg·m^{-3}	T[b] /K	p[c] /MPa	ρ /kg·m^{-3}	$t_{95}(df_\rho)$[d]	$U(\rho)$[e] /kg·m^{-3}
		Run 1					**Run 2**		
270.00	30.002	1440.19	2.12	0.61	270.00	29.983	1440.06	2.12	0.71
270.00	25.006	1429.41	2.11	0.62	270.00	24.997	1429.31	2.11	0.76
270.00	20.009	1417.85	2.09	0.64	270.00	20.011	1417.77	2.09	0.81
270.00	15.009	1405.33	2.07	0.66	270.00	15.010	1405.24	2.06	0.83
270.00	10.008	1391.64	2.05	0.69	270.00	10.010	1391.55	2.05	0.87
270.00	5.010	1376.49	2.03	0.73	270.00	5.009	1376.41	2.03	0.87
270.00	3.009	1369.93	2.03	0.74	270.00	3.010	1369.84	2.03	0.61
270.00	1.011	1363.00	2.02	0.77	270.00	1.010	1362.92	2.02	0.63
270.00	0.510	1361.20	2.02	0.77	270.00	0.512	1361.16	2.02	0.67
290.00	29.997	1398.69	2.10	0.62	290.00	29.993	1398.65	2.10	0.74
290.00	25.010	1386.32	2.09	0.64	290.00	25.009	1386.29	2.09	0.79
290.00	20.010	1372.83	2.07	0.66	290.00	20.012	1372.80	2.07	0.88
290.00	15.011	1358.04	2.05	0.68	290.00	15.011	1357.98	2.05	0.93
290.00	10.010	1341.54	2.03	0.72	290.00	10.008	1341.49	2.03	0.97
290.00	5.011	1322.80	2.01	0.78	290.00	5.008	1322.73	2.01	0.98
290.00	3.010	1314.47	2.01	0.81	290.00	3.009	1314.41	2.01	0.63
290.00	1.008	1305.55	2.00	0.85	290.00	1.010	1305.51	2.00	0.66
290.00	0.511	1303.23	2.00	0.85	290.00	0.509	1303.17	2.00	0.70
310.00	29.999	1357.88	2.09	0.62	310.00	29.996	1357.81	2.09	0.79
310.00	25.009	1343.61	2.07	0.64	310.00	25.009	1343.54	2.07	0.87
310.00	20.008	1327.84	2.05	0.67	310.00	20.009	1327.78	2.05	1.00
310.00	15.011	1310.24	2.03	0.70	310.00	15.012	1310.17	2.03	1.22
310.00	10.010	1290.12	2.02	0.76	310.00	10.010	1290.05	2.02	0.76
310.00	5.010	1266.45	2.00	0.84	310.00	5.011	1266.40	2.00	0.85
310.00	3.012	1255.60	2.00	0.90	310.00	3.010	1255.54	2.00	0.90
310.00	1.010	1243.65	1.99	0.96	310.00	1.009	1243.62	1.99	0.95
310.00	0.510	1240.47	1.99	0.97	310.00	0.508	1240.43	1.99	0.97
330.00	29.991	1316.90	2.07	0.62	370.00	29.993	1234.33	2.06	0.63
330.00	26.005	1303.89	2.06	0.65	370.00	25.996	1217.09	2.04	0.66
330.00	22.004	1289.64	2.04	0.67	370.00	21.997	1197.75	2.02	0.70
330.00	18.013	1273.95	2.03	0.71	370.00	17.995	1175.56	2.01	0.75
330.00	14.012	1256.33	2.02	0.75	370.00	13.999	1149.49	2.00	0.83
330.00	10.010	1236.14	2.00	0.82	370.00	9.996	1117.27	1.99	0.96
330.00	6.010	1212.33	1.99	0.92	370.00	5.996	1074.25	1.98	1.19
330.00	2.010	1182.70	1.99	1.07					
330.00	1.009	1173.90	1.99	1.13					

Table 2. Continued.

T[b] /K	p[c] /MPa	ρ /kg·m^{-3}	$t_{95}(df_\rho)$[d]	$U(\rho)$[e] /kg·m^{-3}	T[b] /K	p[c] /MPa	ρ /kg·m^{-3}	$t_{95}(df_\rho)$[d]	$U(\rho)$[e] /kg·m^{-3}
Run 1					**Run 2**				
350.00	30.008	1275.69	2.06	0.63					
350.00	25.994	1260.63	2.05	0.65					
350.00	21.991	1244.01	2.03	0.68					
350.00	17.993	1225.38	2.02	0.73					
350.00	14.014	1204.10	2.01	0.79					
350.00	10.009	1178.78	2.00	0.87					
350.00	6.012	1147.38	1.99	1.03					
350.00	2.011	1104.36	1.98	1.31					
350.00	1.510	1097.54	1.98	1.36					
370.00	30.008	1234.73	2.06	0.63					
370.00	26.007	1217.55	2.04	0.66					
370.00	21.999	1197.88	2.02	0.70					
370.00	18.009	1175.72	2.01	0.75					
370.00	14.012	1149.60	2.00	0.83					
370.00	10.011	1117.41	1.99	0.95					
370.00	6.008	1074.39	1.98	1.19					
370.00	2.011	1003.83	1.98	1.80					
390.00	30.001	1193.51	2.05	0.63					
390.00	25.999	1173.66	2.03	0.66					
390.00	22.008	1151.10	2.02	0.71					
390.00	18.008	1124.72	2.00	0.77					
390.00	14.010	1092.66	1.99	0.88					
390.00	10.010	1051.10	1.99	1.05					
390.00	6.009	989.33	1.98	1.42					
390.00	4.506	953.61	1.98	1.73					
410.00	30.007	1151.97	2.05	0.67					
410.00	25.993	1129.41	2.03	0.72					
410.00	22.008	1103.42	2.01	0.79					
410.00	18.009	1072.16	2.00	0.91					
410.00	14.009	1032.78	1.99	1.14					
410.00	10.008	978.49	1.98	0.54					

[a]Reported values are averages of ten replicate measurements at each (T, p) state point.
[b]Standard uncertainty in temperature is ~ 15 mK.
[c]Standard uncertainty in pressure is ~ 5 kPa.
[d]Coverage factor from the *t*-distribution for df_ρ degrees of freedom and a 95% confidence level.
[e]Combined, expanded (95% confidence level) uncertainty in density.

3.2 Vapor Pressure

Measured vapor pressures (p_{sat}) for R-1336yf are shown in Fig. 3, plotted as pressure vs temperature. In this figure, no distinction is made between the two sets of measurements (‘Run

1' and 'Run 2'). The p_{sat} data shown in Fig. 3 are also reported in Table 3, along with the combined expanded (k = 2) uncertainty ($U(p_{\mathrm{sat}})$) and the corresponding relative combined expanded uncertainty ($100 \cdot U(p_{\mathrm{sat}})/p_{\mathrm{sat}}$). Here, $U(p_{\mathrm{sat}})$ is calculated using an expression similar to that shown in Eq. 6, except in this case the coverage factor is k and is equal to 2 for all points. Determination of the combined standard uncertainty in vapor pressure ($u(p_{\mathrm{sat}})$) is discussed in Sec. 3.4.2. Note that the reported values are averages of 10 replicate measurements at each temperature.

Table 3. Measured Temperature (T) and Vapor Pressure (p_{sat}) Data for R-1336yf.[a]

T[b] /K	p_{sat} /kPa	$U(p_{\mathrm{sat}})$[c] /kPa	$100 \cdot U(p_{\mathrm{sat}})/p_{\mathrm{sat}}$[d]
		Run 1	
265.00	68.20	0.40	0.59
265.00	68.30	0.40	0.59
270.00	84.20	0.42	0.50
275.00	102.90	0.46	0.45
275.00	103.00	0.46	0.44
280.00	124.80	0.49	0.40
285.00	150.20	0.55	0.37
285.00	150.20	0.55	0.37
290.00	179.40	0.61	0.34
295.00	212.80	0.70	0.33
295.00	212.80	0.70	0.33
300.00	248.40	0.80	0.32
305.00	291.20	0.92	0.32
305.00	291.40	0.92	0.32
310.00	339.60	1.07	0.31
315.00	392.80	1.23	0.31
315.00	393.30	1.23	0.31
320.00	453.10	1.43	0.31
325.00	520.30	1.65	0.32
325.00	520.90	1.65	0.32
		Run 2	
265.00	68.30	0.40	0.59
275.00	103.00	0.46	0.44
285.00	150.20	0.55	0.37
295.00	212.80	0.70	0.33
305.00	291.40	0.92	0.32
315.00	393.30	1.23	0.31
325.00	520.90	1.65	0.32
335.00	677.30	2.19	0.32
345.00	866.70	2.89	0.33
355.00	1093.20	3.78	0.35

[a]Reported values are averages of ten measurements at each temperature.
[b]Standard uncertainty in temperature is ~ 20 mK.
[c]Combined expanded (k = 2) uncertainty in vapor pressure.
[d]Relative combined expanded (k = 2) uncertainty in vapor pressure.

3.3 Speed of Sound

The measured speed of sound (w) data for R-1336yf are shown in Figs. 5a and 5b, plotted vs temperature and pressure, respectively. In this figure, different pseudo-isochores are indicated by different colored open square symbols. The corresponding average densities, which were calculated using the EOS developed as part of this work, are listed next to each symbol in the legend. It should be noted that only every other pseudo-isochore has been plotted to avoid visual clutter. The complete set of measured sound speed data is reported in Table 4, along with the relative combined expanded uncertainty ($100 \cdot U(w)/w$). As was the case with p_{sat}, $U(\mathrm{w})$ is calculated using an expression similar to that shown in Eq. 6, but with a coverage factor k that is equal to 2 for all points. Determination of the combined standard uncertainty in speed of sound ($u(w)$) is discussed in Sec. 3.4.3. Note that the reported values are averages of up to 12 replicate measurements at each (T, p) state point.

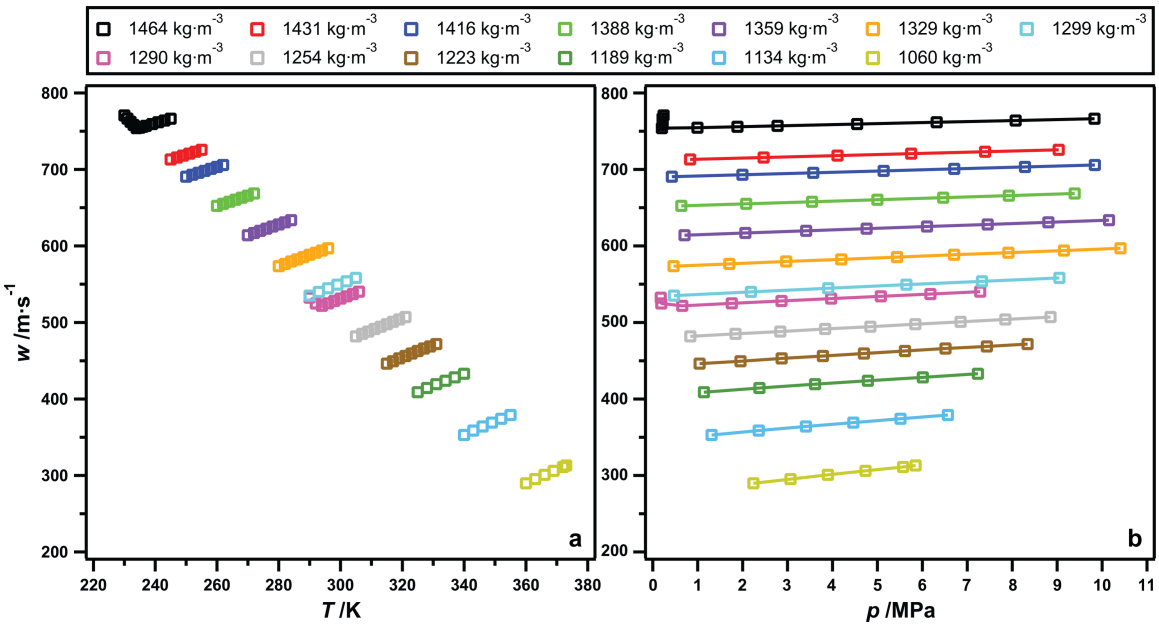

Fig. 5. Measured speed of sound data for R-1336yf, plotted as a function of temperature (a) and pressure (b). Symbols represent experimental data points; lines are drawn to guide the eye. Only every other pseudo-isochore is plotted to avoid visual clutter. Corresponding average densities were calculated using the new EOS developed as part of this work.

Table 4. Measured Temperature (T), Pressure (p), and Speed of Sound (w) Data for R-1336yf.[a]

T[b] /K	p[c] /MPa	w /m·s^{-1}	$100 \cdot U(w)/w$[d]	T[b] /K	p[c] /MPa	w /m·s^{-1}	$100 \cdot U(w)/w$[d]
230.000	0.238	770.62	0.28	299.967	0.698	499.40	0.52
231.001	0.218	766.46	0.29	301.966	1.743	502.63	0.50
232.001	0.216	762.31	0.29	303.968	2.821	506.08	0.49
233.003	0.218	758.18	0.29	305.973	3.847	509.07	0.47
233.990	0.202	754.00	0.29	307.974	4.917	512.35	0.46
234.994	0.994	754.61	0.29	309.975	5.948	515.34	0.45
235.997	1.885	755.78	0.29	311.986	6.995	518.34	0.43
237.000	2.778	756.98	0.29	313.980	8.047	521.44	0.42
238.992	4.549	759.37	0.28	315.987	9.082	524.29	0.41
241.002	6.320	761.69	0.28				
242.997	8.077	764.02	0.27	304.978	0.836	481.81	0.54
244.992	9.833	766.37	0.27	306.980	1.842	485.15	0.52
				308.965	2.838	488.39	0.51
239.997	0.903	733.72	0.30	310.970	3.837	491.55	0.49
241.991	2.594	736.07	0.30	312.982	4.844	494.72	0.48
244.002	4.297	738.44	0.29	314.975	5.843	497.84	0.46
245.999	5.997	740.86	0.29	316.984	6.851	500.96	0.45
248.003	7.694	743.28	0.28	318.977	7.848	503.98	0.44
250.001	9.388	745.68	0.28	320.990	8.854	507.00	0.43
244.993	0.831	713.13	0.32	309.975	0.975	464.40	0.56
246.992	2.467	715.59	0.31	312.981	2.415	469.43	0.54
248.995	4.111	718.10	0.31	315.986	3.859	474.38	0.51
250.992	5.752	720.62	0.30	318.977	5.299	479.21	0.49
252.991	7.397	723.16	0.30	321.991	6.743	483.93	0.47
254.995	9.036	725.67	0.29	324.984	8.179	488.53	0.45
250.001	0.437	690.53	0.33	314.974	1.041	446.16	0.59
251.999	2.006	693.07	0.33	316.982	1.951	449.54	0.57
254.000	3.583	695.65	0.32	318.977	2.868	452.92	0.55
255.990	5.148	698.21	0.32	320.990	3.785	456.24	0.54
257.993	6.721	700.78	0.31	322.990	4.699	459.47	0.52
259.987	8.282	703.30	0.30	324.984	5.611	462.69	0.50
261.981	9.857	705.93	0.30	326.980	6.516	465.76	0.49
				328.977	7.435	468.93	0.48
249.999	0.424	690.46	0.33	330.978	8.340	471.91	0.46
251.998	1.995	693.01	0.33				
253.998	3.573	695.60	0.32	319.973	1.099	427.85	0.62
255.989	5.138	698.16	0.32	322.987	2.403	432.99	0.59
257.993	6.711	700.72	0.31	325.983	3.707	438.03	0.56
259.994	8.283	703.30	0.30	328.978	5.008	442.93	0.54
261.980	9.840	705.83	0.30	331.977	6.318	447.78	0.51
				334.976	7.556	451.81	0.49

Table 4. Continued.

T[b] /K	p[c] /MPa	w /m·s^{-1}	$100 \cdot U(w)/w$[d]	T[b] /K	p[c] /MPa	w /m·s^{-1}	$100 \cdot U(w)/w$[d]
254.992	0.667	672.30	0.35				
257.992	2.939	676.21	0.34	324.983	1.137	409.11	0.66
260.985	5.211	680.15	0.33	327.977	2.374	414.38	0.62
263.988	7.480	684.04	0.32	330.977	3.611	419.49	0.59
266.975	9.739	687.92	0.31	333.976	4.787	423.77	0.57
				336.979	6.010	428.44	0.54
259.992	0.635	652.39	0.36	339.974	7.236	433.08	0.52
261.980	2.079	655.02	0.35				
263.987	3.543	657.73	0.35	329.976	1.002	387.75	0.71
265.979	4.999	660.42	0.34	332.974	2.113	392.42	0.67
267.986	6.464	663.11	0.33	335.977	3.272	397.55	0.64
269.982	7.926	665.83	0.33	338.969	4.431	402.56	0.60
271.980	9.391	668.56	0.32	341.986	5.603	407.52	0.57
				344.987	6.769	412.31	0.55
264.984	0.552	632.27	0.38				
266.974	1.950	635.04	0.37	339.974	1.309	353.01	0.79
268.982	3.361	637.84	0.36	342.975	2.359	358.62	0.74
270.979	4.763	640.60	0.35	345.977	3.409	364.00	0.70
272.984	6.163	643.31	0.35	348.984	4.461	369.19	0.66
274.974	7.556	646.03	0.34	351.992	5.514	374.21	0.63
276.971	8.953	648.74	0.33	355.002	6.568	379.10	0.60
269.979	0.705	614.06	0.39	349.991	1.715	319.91	0.88
271.979	2.060	616.93	0.38	352.999	2.648	325.56	0.82
273.976	3.413	619.78	0.37	355.995	3.578	330.92	0.77
275.972	4.761	622.60	0.37	359.011	4.520	336.19	0.73
277.972	6.104	625.34	0.36	362.007	5.458	341.26	0.69
279.980	7.454	628.12	0.35	365.009	6.396	346.15	0.65
281.985	8.804	630.88	0.34				
283.973	10.154	633.68	0.34	360.002	2.239	289.70	0.97
				363.001	3.065	295.37	0.91
274.974	0.510	593.22	0.41	366.006	3.898	300.82	0.85
277.971	2.440	597.51	0.40	369.011	4.733	306.06	0.79
280.984	4.388	601.84	0.38	372.021	5.571	311.12	0.75
283.971	6.329	606.17	0.37	373.019	5.850	312.75	0.73
286.981	8.280	610.47	0.36				
289.981	10.209	614.62	0.35	274.967	0.593	593.99	0.41
				277.965	2.499	598.01	0.40
279.978	0.463	573.54	0.43	280.977	4.428	602.19	0.38
281.984	1.702	576.49	0.42	283.965	6.357	606.42	0.37
283.971	2.969	579.68	0.41	286.975	8.301	610.67	0.36
285.976	4.194	582.52	0.40	289.973	10.260	615.02	0.35
287.986	5.436	585.41	0.39				

Table 4. Continued.

T[b] /K	p[c] /MPa	w /m·s^{-1}	$100 \cdot U(w)/w$[d]	T[b] /K	p[c] /MPa	w /m·s^{-1}	$100 \cdot U(w)/w$[d]
289.980	6.708	588.53	0.38	289.974	0.471	535.32	0.47
291.972	7.915	591.22	0.37	292.969	2.185	540.05	0.45
293.979	9.152	594.02	0.36	295.971	3.904	544.71	0.44
295.975	10.411	597.01	0.36	298.975	5.645	549.46	0.42
				301.962	7.328	553.78	0.40
284.973	0.398	553.80	0.45	304.974	9.051	558.24	0.39
287.985	2.186	558.37	0.44				
290.982	3.976	562.93	0.42	294.962	0.864	520.10	0.49
293.979	5.759	567.40	0.40	297.968	2.526	524.94	0.47
296.983	7.542	571.79	0.39	300.970	4.166	529.55	0.45
299.969	9.312	576.09	0.37	303.964	5.826	534.26	0.43
				306.978	7.487	538.81	0.41
289.978	0.177	532.46	0.48	309.972	9.109	543.10	0.40
291.970	0.190	524.91	0.49				
293.979	0.655	521.76	0.49				
295.975	1.759	524.94	0.47				
297.972	2.864	528.09	0.46				
299.969	3.971	531.22	0.45				
301.966	5.074	534.29	0.44				
303.969	6.179	537.31	0.43				
305.973	7.286	540.33	0.41				

[a]Reported values are averages of up to twelve measurements at each (T, p) state point. Isochores are separated by breaks and are listed in the order measurements were made (generally in order of decreasing density).
[b]Standard uncertainty in temperature is ~ 5 mK.
[c]Standard uncertainty in pressure is ~ 7 kPa.
[d]Relative combined expanded (k = 2) uncertainty in speed of sound.

3.4 Measurement Uncertainty

3.4.1 Density Uncertainty

The main sources of uncertainty for the density data collected with the VTD are the uncertainties associated with the temperature and pressure measurements, the uncertainty associated with the instrument calibration, and the uncertainty associated with the sample composition. Therefore, $u(\rho)$ can be expressed as

$$u(\rho) = \sqrt{u_T(\rho)^2 + u_p(\rho)^2 + u_{\mathrm{cal}}(\rho)^2 + u_x(\rho)^2} \quad (7)$$

where the combined standard uncertainties due to temperature ($u_T(\rho)$), pressure ($u_p(\rho)$), instrument calibration ($u_{\mathrm{cal}}(\rho)$), and sample composition ($u_x(\rho)$) are all in units of kg·m^{-3}. Determination of each of these uncertainty components follows the methods discussed in detail in Fortin and Outcalt [19]. In this work, estimated combined standard uncertainty in temperature was 15 mK, which corresponds to $u_T(\rho)$ = 0.04 kg·m^{-3}. Similarly, an estimated

combined uncertainty in pressure of 5 kPa corresponds to $u_p(\rho)$ = 0.02 kg·m^{-3}. Finally, $u_{\mathrm{cal}}(\rho)$ was approximately 0.2 kg·m^{-3} while $u_x(\rho)$ varied with temperature and pressure and ranged from approximately 0.2 kg·m^{-3} to 0.9 kg·m^{-3}.

As was discussed in Sec. 3.1, the combined expanded uncertainty in density, $U(\rho)$, was calculated according to Eq. 6 using the $u(\rho)$ values calculated with Eq. 7 and the coverage factor, $t_{95}(df_\rho)$. The corresponding degrees of freedom, df_ρ, was calculated using the Welch-Satterthwaite approximation [20]:

$$df_\rho = \frac{u(\rho)^4}{\left(\frac{u_T(\rho)^4}{df_T}+\frac{u_p(\rho)^4}{df_p}+\frac{u_{\mathrm{cal}}(\rho)^4}{df_{\mathrm{cal}}}+\frac{u_x(\rho)^4}{df_x}\right)} \tag{8}$$

where df_T, df_p, df_{cal}, and df_x are the corresponding degrees of freedom for $u_T(\rho)$, $u_p(\rho)$, $u_{\mathrm{cal}}(\rho)$, and $u_x(\rho)$ respectively. In this work, $t_{95}(df_\rho)$ ranged from 1.98 to 2.12 and $U(\rho)$ ranged from 0.54 kg·m^{-3} to 1.80 kg·m^{-3}, corresponding to relative combined expanded uncertainties of approximately 0.04 % to 0.18 %.

3.4.2 Vapor Pressure Uncertainty

The uncertainty analysis for the R-1336yf p_{sat} measurements followed the procedure described in detail in Rowane and Outcalt [21] but with a few differences. First, given the lower purity of the measurement sample in this work, the uncertainty contribution associated with sample composition had to be reevaluated. Here, standard uncertainty associated with composition increased with temperature and was estimated to range from 0.2 kPa at 265 K to 2.2 kPa at 360 K. Second, because no independent EOS for R-1336yf existed when these measurements were being made, the saturated liquid densities needed for the head pressure correction at temperatures above 296 K were obtained from the EOS for R-236fa (1,1,1,3,3,3-hexafluoropropane) [22] included in REFPROP (version 10.0) [15]. R-236fa was chosen for this purpose because the molecular simulation work of Raabe [6] indicated that the two fluids might exhibit similar properties. In this work, $U(p_{\mathrm{sat}})$ ranged from 0.40 kPa to 4.31 kPa, corresponding to relative combined expanded uncertainties of approximately 0.31 % to 0.59 %.

3.4.3 Speed of Sound Uncertainty

The uncertainty analysis for the R-1336yf speed of sound measurements followed the procedure described in detail in McLinden and Perkins [10] and included contributions from temperature, pressure, sample purity, the path length calibration with propane, and the standard deviation in the measured speed of sound. That last component was used to estimate the uncertainty in Δt in Eq. 5. In previous studies, relative combined expanded uncertainties in measured speeds of sound were as low as 0.036 %. However, the low purity of the R-1336yf sample used in this work required an additional estimate of uncertainty due to sample composition thereby raising the lowest reported uncertainty to 0.27 %. Overall, the relative combined expanded uncertainties ranged from approximately 0.27 % to 0.97 %, corresponding to $U(w)$ values ranging from 2.1 m·s^{-1} to 2.8 m·s^{-1}. As was observed with the vapor pressure

measurements, the uncertainty increased as a function of temperature. Additionally, as described in Rowane and Rasmussen [18], higher uncertainties occurred at temperatures and pressures approaching the critical point where the echo signals were much weaker and the speed of sound rapidly changes with pressure.

4. Equation of State

4.1 The Helmholtz EOS

The equation of state is expressed in terms of the Helmholtz energy as a function of temperature and density. The form of the equation is

$$\frac{a(T,\rho)}{RT} = \alpha(\tau,\delta) = \alpha^{\mathrm{o}}(\tau,\rho) + \alpha^{\mathrm{r}}(\tau,\rho), \tag{9}$$

where a is the molar Helmholtz energy, α is the dimensionless Helmholtz energy, R is the molar gas constant, $\tau = T_{\mathrm{c}}/T$ is the reciprocal reduced temperature, T_{c} is the critical temperature, $\delta = \rho/\rho_{\mathrm{c}}$ is the reduced density, and ρ_{c} is the critical density [23]. The dimensionless Helmholtz energy in Eq. 9 is comprised of an ideal-gas contribution, α^{o}, and a residual contribution, α^{r}. Fluid-specific parameters and physical constants associated with the development of this equation are reported in Table 5.

Table 5. Constants and Fluid-Specific Parameters for R-1336yf.

Symbol	Quantity	Value	Unit	Reference
R	Molar gas constant	8.314462618	J·mol^{-1}·K^{-1}	[24]
M	Molar mass	164.0490992	g·mol^{-1}	[25]
T_{c}	Critical temperature	411.02	K	This work
p_{c}	Critical pressure	3167.06	kPa	This work
ρ_{c}	Critical density	3.05	mol·dm^{-3}	This work
T_{nbp}	Normal boiling point temperature	275.34	K	This work
T_{tp}	Triple-point temperature	195.0	K	[26]
ω	Acentric factor	0.2885		This work
μ	Dipole moment	2.2	D	This work

Thermodynamic properties are found from taking derivatives of the Helmholtz energy in Eq. 9, as discussed in Lemmon and Jacobsen [23]. Some particularly useful expressions are

$$p = \rho RT\left[1 + \delta\left(\frac{\partial\alpha^{\mathrm{r}}}{\partial\delta}\right)_{\tau}\right], \tag{10}$$

$$\frac{h}{RT} = \tau\left[\left(\frac{\partial\alpha^{\mathrm{o}}}{\partial\tau}\right)_{\delta} + \left(\frac{\partial\alpha^{\mathrm{r}}}{\partial\tau}\right)_{\delta}\right] + \delta\left(\frac{\partial\alpha^{\mathrm{r}}}{\partial\delta}\right)_{\tau} + 1, \tag{11}$$

$$\frac{c_v}{R} = -\tau^2\left[\left(\frac{\partial^2\alpha^{\mathrm{o}}}{\partial\tau^2}\right)_{\delta} + \left(\frac{\partial^2\alpha^{\mathrm{r}}}{\partial\tau^2}\right)_{\delta}\right], \tag{12}$$

and

$$B(T) = \lim_{\delta \to 0} \left[\frac{1}{\rho_c} \left(\frac{\partial \alpha^r}{\partial \delta} \right)_\tau \right], \quad (13)$$

where p is the pressure, h is the molar enthalpy, c_v is the isochoric heat capacity, and B is the second virial coefficient [23]. Additional expressions are given by Lemmon and Jacobsen [23].

The ideal-gas Helmholtz energy, α^o, is given by the expression,

$$\alpha^o(\tau, \delta) = \frac{h_0^o \tau}{R T_c} - \frac{s_0^o}{R} - 1 + \ln \frac{\delta \tau_0}{\delta_0 \tau} - \frac{\tau}{R} \int_{\tau_0}^{\tau} \frac{c_p^o}{\tau^2} \mathrm{d}\tau + \frac{1}{R} \int_{\tau_0}^{\tau} \frac{c_p^o}{\tau} \mathrm{d}\tau, \quad (14)$$

where $\tau_0 = T_c/T_0$, $\delta_0 = \rho_0/\rho_c = p_0/(RT_0\rho_c)$, T_0 is a reference-state temperature, p_0 is a reference pressure for the ideal gas, and ρ_0 is the ideal-gas density at T_0 and p_0.

In Eq. 14 it is necessary to have the ideal-gas heat capacity (c_p^o). Experimental data were unavailable, so we used computational chemistry to obtain values for the ideal-gas heat capacity that were incorporated into the multiproperty fitting process. Ideal-gas heat capacities were computed based on the results of hybrid Density Functional Theory (DFT) B3LYP-D3(BJ)/def2-TZVP [27, 28] and double hybrid DFT revDSD-PBEP86-D3(BJ)/def2QZVPD [29, 30] calculations. For B3LYP-D3(BJ)/def2-TZVP, vibrational frequency scaling was 0.96 for hydrogen stretches and 0.985 for the rest [31]. For revDSD-PBEP86-D3(BJ)/def2QZVPD, a unity scaling factor was assumed [32]. CF_3- and CH_2CF- tops were treated as independent one-dimensional hindered rotors in both cases. The rotational scans for both were performed at B3LYP-D3(BJ)/def2-TZVP level, and the energies were subsequently refined with single-point LCCSD(T)/aug-cc-pVQZ [32-34] calculations. DFT calculations were performed with Gaussian 16 software [35] and LCCSD(T) energies were computed with the MRCC package [36]. For the temperature range considered, 100 K to 1000 K, the two DFT models agree within 1.4 J·mol^{-1}·K^{-1} and within the NIST ThermoData Engine (TDE)-estimated uncertainties of 10 % [37]. The TDE calculations [37] were made with a NIST-modified Joback group contribution method [38]. The small difference in DFT models is probably within the anticipated uncertainty ($\gtrsim$ 2 J·mol^{-1}·K^{-1}). For the final recommendation, the higher-level revDSD-PBEP86-D3(BJ)/def2-QZVPD model (Table 6) was chosen. The results for these two models, as well as the group-contribution estimates from TDE [37], are shown in Fig. 6.

Table 6. Ideal-Gas Heat Capacity (c_p^o) as a Function of Temperature (T) for R-1336yf.[a]

T /K	c_p^o /J·mol^{-1}·K^{-1}	T /K	c_p^o /J·mol^{-1}·K^{-1}
100	70.3047	560	201.8019
120	78.8738	580	204.5440
140	87.4904	600	207.1326
160	95.9637	620	209.5784
180	104.1810	640	211.8916
200	112.0836	660	214.0814
220	119.6463	680	216.1566
240	126.8628	700	218.1251
260	133.7356	720	219.9943
280	140.2710	740	221.7710
298.15	145.9160	760	223.4616
300	146.4764	780	225.0717
320	152.3600	800	226.6067
340	157.9304	820	228.0714
360	163.1970	840	229.4703
380	168.1704	860	230.8075
400	172.8618	880	232.0868
420	177.2836	900	233.3117
440	181.4486	920	234.4853
460	185.3702	940	235.6106
480	189.0622	960	236.6903
500	192.5380	980	237.7271
520	195.8113	1000	238.7231
540	198.8951		

[a]Calculated using the revDSD-PBEP86-D3(BJ)/def2-QZVPD model.

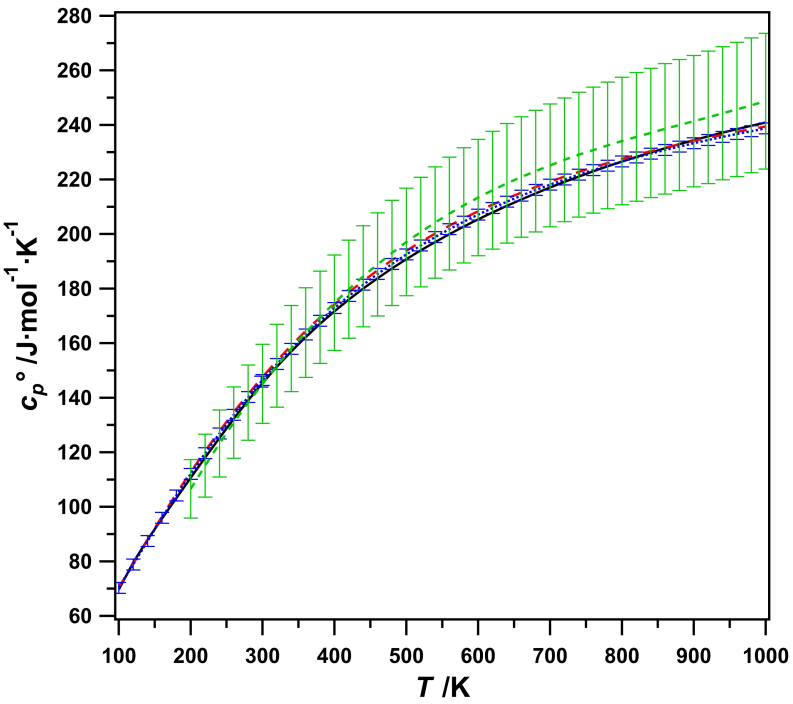

Fig. 6. Calculated ideal-gas heat capacities for R-1336yf. Shown are results for calculations using Eq. 15 (──), B3LYP-D3(BJ)/def2-TZVP (– –), revDSD-PBEP86-D3(BJ)/def2-QZVPD (·····), and TDE Joback (- - -). Error bars representing the estimated expanded (k = 2) uncertainty are included for the revDSD-PBEP86-D3(BJ)/def2-QZVPD (~ 2 J·mol^{-1}·K^{-1}) and TDE Joback values (10.7 – 24.9 J·mol^{-1}·K^{-1}).

Finally, although it is not directly incorporated into the EOS, we computed the dipole moment at 298.15 K by Gibbs-averaging of the corresponding values for three conformers of R-1336yf (rotamers of CH_2CF- torsion) computed at B3LYP-D3(BJ)/def2-TZVP level; the value we obtained was 2.2 D.

We included these values into the multiproperty fitting procedure and obtained the following equation

$$\frac{c_p^o}{R} = n_0^o + \sum_{i=1}^{3} n_i^o \left(\frac{m_i^o}{T}\right)^2 \frac{\exp(m_i^o/T)}{[\exp(m_i^o/T)-1]^2}, \qquad (15)$$

where the coefficients n_i^o and the exponents m_i^o are presented in Table 7. Values computed with Eq. 15 are shown in Fig. 6 and are mostly within the uncertainty band of the computational chemistry results, approximately 2 J·mol^{-1}·K^{-1}.

Table 7. Coefficients for Eqs. 15 and 16.

i	n_i^o	m_i^o
0	4	
1	9.529	318 K
2	14.083	1137 K
3	6.385	3221 K
4	-14.75787030085678	
5	10.2338799972408516	

The ideal-gas Helmholtz energy derived from Eqs. 14 and 15 may be written as

$$\alpha^{o}(\tau,\delta) = \ln\delta + n_4^o + n_5^o\tau + (n_0^o - 1)\ln\tau + \sum_{i=1}^{3} n_i^o \ln\left[1 - \exp\left(-\frac{m_i^o\tau}{T_c}\right)\right] \quad (16)$$

with n_i^o and m_i^o given in Table 7. These values were determined according to the convention of the International Institute of Refrigeration (IIR) that the specific enthalpy and entropy of the saturated liquid state at 0 °C are 200 kJ·kg^{-1} and 1 kJ·kg^{-1}·K^{-1}, respectively. The large number of digits in n_4^o and n_5^o are necessary to accurately reproduce the reference-state values.

The residual Helmholtz energy is often fit to the following empirical equation

$$\alpha^{r}(\tau,\delta) = \sum_{i=1}^{K_1} n_i\tau^{t_i}\delta^{d_i} + \sum_{i=K_1+1}^{K_2} n_i\tau^{t_i}\delta^{d_i}\exp(-g_i\delta^{e_i}) + \sum_{i=K_2+1}^{K_3} n_i\tau^{t_i}\delta^{d_i}\exp[-\eta_i(\delta-\varepsilon_i)^2 - \beta_i(\tau-\gamma_i)^2], \quad (17)$$

where the number of terms K_1, K_2, and K_3 and values of the coefficients n_i, exponents t_i and d_i, parameters g_i and e_i, and Gaussian parameters η_i, ε_i, β_i, and γ_i, are determined by fitting experimental data in a multiproperty fitting procedure that incorporates a variety of fluid properties such as the density, vapor pressure, critical parameters, heat capacities, and the speed of sound [23]. The first set of terms are polynomials, the second set contains exponentials, and the third set are often called the Gaussian bell-shaped terms. In this work, following the recent work of Akasaka and Lemmon [39] and Huber et al. [40], we modified the Gaussian term such that β_i = 0, resulting in the simpler expression

$$\alpha^{r}(\tau,\delta) = \sum_{i=1}^{K_1} n_i\tau^{t_i}\delta^{d_i} + \sum_{i=K_1+1}^{K_2} n_i\tau^{t_i}\delta^{d_i}\exp(-g_i\delta^{e_i}) + \sum_{i=K_2+1}^{K_3} n_i\tau^{t_i}\delta^{d_i}\exp[-\eta_i(\delta-\varepsilon_i)^2]. \quad (18)$$

The regression procedure utilized an in-house nonlinear least-squares algorithm developed by Lemmon and coworkers [17, 23]. We follow the procedure described by Lemmon et al. [17] and more recently summarized by Akasaka and Lemmon [39, 41, 42]. The resulting parameters are given in Table 8. The large number of digits in n_5 and n_6 are required to satisfy the critical-point conditions.

Table 8. Coefficients for the Residual Part of the Helmholtz Energy (Eq. 18).

i	n_i	t_i	d_i	e_i	g_i	η_i	ε_i
1	0.0293023	1	4				
2	0.54634	0.154	1				
3	0.051	0.2275	2				
4	0.146	0.455	3				
5	-0.1140088219803	0.75	1				
6	-0.9899987857495	1.176	2				
7	-0.383	1.14	1	1	2.55		
8	-0.83	1.34	1	2	0.996		
9	-0.091	6.3	1	3	0.719		
10	-0.01078	6.5	2	3	2.7955		
11	-0.03861	4.9	3	3	0.294		
12	-0.224	1.6	1			2.34	-0.075
13	-0.04161	1.5	2			1.216	1.12
14	-0.24598	1.4	1			4.115	-0.328
15	-0.1595	1.45	1			1.391	0.912

In addition, in order to determine the saturation conditions, the Maxwell criterion [43] is applied. This is an iterative process and can be computationally expensive. To speed up these calculations, ancillary equations for the vapor pressure and the saturated liquid and saturated vapor densities were developed to provide accurate starting guesses for iterative procedures. The equation for vapor pressure p_{sat} is

$$\ln\left(\frac{p_{\mathrm{sat}}}{p_{\mathrm{c}}}\right) = \left(\frac{T_{\mathrm{c}}}{T}\right)\sum_{i=1}^{5} n_i \left(1-\frac{T}{T_{\mathrm{c}}}\right)^{t_i}, \tag{19}$$

and the equations for saturated liquid density ρ' and saturated vapor density ρ'' are

$$\frac{\rho'}{\rho_{\mathrm{c}}} = 1 + \sum_{i=1}^{6} n_i \left(1-\frac{T}{T_{\mathrm{c}}}\right)^{t_i}, \tag{20}$$

and

$$\frac{\rho''}{\rho_{\mathrm{c}}} = \sum_{i=1}^{6} n_i \left(1-\frac{T}{T_{\mathrm{c}}}\right)^{t_i}. \tag{21}$$

The values of the parameters for the ancillary equations are given in Table 9. These values may be used to estimate starting values, but for the actual calculation of vapor-liquid equilibrium the full EOS subject to the Maxwell criterion should be used. Deviations of Eqs. 19 - 21 from the saturation boundary as calculated from the EOS with the Maxwell criterion are shown in Fig. 7, where X denotes the property (i.e., vapor pressure, saturated liquid density, or saturated vapor density). Test values for checking the computer implementation of the full EOS are provided in

Table 10 and sample Python code to reproduce the values is provided in Appendix A (Supporting Information).

Table 9. Ancillary Equation Coefficients.

	Vapor Pressure (Eq. 19)		Saturated Liquid Density (Eq. 20)		Saturated Vapor Density (Eq. 21)	
i	n_i	t_i	n_i	t_i	n_i	t_i
1	-6.70620412	1	1.89704145	0.4638665	-0.63919655	0.3596694
2	-0.14734195	1.5	156.14843903	1.4048242	-7.01618604	0.7965149
3	-125.28818422	5.6772434	-385.3512708	1.6191201	-26.08309983	3.1260808
4	-135.11656438	6.9682299	452.87277179	2.0080574	-88.81569661	7.1923894
5	244.94512747	6.2992649	-388.79185571	2.4908164	-73.60633017	13.7221417
6			167.77897546	2.8199018	-268.15824395	18.2627862

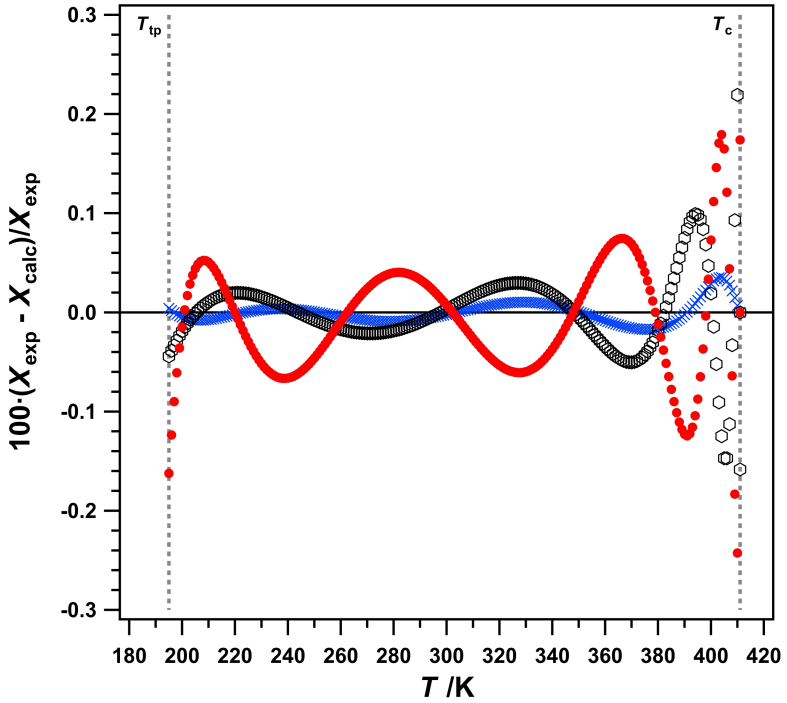

Fig. 7. Relative deviations of the ancillary equations (Eqs. 19 – 21) from the saturation boundary as calculated using the Maxwell solution of the EOS. Here, X denotes the property: vapor pressure (×), saturated liquid density (⬡), and saturated vapor density (●). The gray dotted lines (⋯) mark the triple-point temperature (T_{tp}) and the critical temperature (T_c).

Table 10. Test Values for the Verification of the Computer Implementation of the R-1336yf EOS.[a]

T /K	ρ /mol·dm^{-3}	p /MPa	w /m·s^{-1}	c_p /J·mol^{-1}·K^{-1}	c_v /J·mol^{-1}·K^{-1}	h /J·mol^{-1}
300	0.00	0.00	126.993	145.382	137.067	61388.4
300	0.01	0.0247198	126.015	146.439	137.704	61304.3
300	8.0	9.81022	580.915	215.800	164.732	39096.1
400	6.0	7.97419	271.765	242.541	180.521	61717.1
400	0.2	0.607417	134.410	178.038	165.839	76387.7

[a] T is temperature, ρ is density, p is pressure, w is speed of sound, c_p is isobaric molar heat capacity, c_v is isochoric molar heat capacity, and h is molar enthalpy.

4.2 Comparisons with Experimental Data

The available thermodynamic data for R-1336yf are summarized in Table 11. Other than the experimental measurements reported in this work, we found only two experimental vapor pressure points in a figure in a patent from 2013 [5]. In addition, there is one literature source that provides molecular simulation data [6].

Also included in Table 11 are the results of comparisons of the EOS with the experimental and simulation data. In addition to the terms previously defined in Eqs. 2–4, we use bias (BIAS) and standard deviation (STDEV) to describe the results of those comparisons, which are defined as

$$\mathrm{BIAS} = \frac{1}{n}\sum_{i=1}^{n} \mathrm{PCT}_i \tag{22}$$

and

$$\mathrm{STDEV} = \sqrt{(\mathrm{PCT}_i - \mathrm{BIAS})^2/n} \tag{23}$$

where n is the number of data points.

The only source of density data are the measurements in this study, all of which are in the liquid phase, covering temperatures from 270 K to 410 K and pressures from 0.5 MPa to 30.0 MPa. Relative deviations of the experimental liquid-phase density data from the EOS calculations are shown in Figs. 8a, 8b, and 8c, plotted as a function of temperature, pressure, and density, respectively. At a level of k = 2, the data are represented by the EOS to within 0.24 %, with an AARD of 0.16 %.

Table 11. Summary of Experimental and Simulated Data for R-1336yf and Comparisons with the EOS.

Source	Pts[a]	Method[b]	$U(X)$[c]	T[d] /K	p[e] /MPa	AARD[f]	BIAS[g]	STDEV[h]	MRD[i]
Single-Phase Density									
This work	101	VTD	0.04–0.18	270–410	0.51–30.01	0.16	0.15	0.12	0.32
Saturated Liquid Density									
Raabe, 2020 [6]	7	Sim	0.1–0.3	278–353	0.10–1.21	1.27	-1.27	0.79	-2.62
Saturated Vapor Density									
Raabe, 2020 [6]	7	Sim	1.7–5.5	278–353	0.10–1.21	12.16	11.41	6.09	16.76
Vapor Pressure									
Robin, 2013 [5]	2	PTx	NA	303	0.27	0.10	0.07	0.10	0.17
Raabe, 2020 [6]	8	Sim	1.2–5.0	274–353	0.10–1.21	11.03	10.48	5.55	15.28
This work	30	VLE	0.31–0.59	265–360	0.07–1.22	1.15	0.82	1.53	4.63
Speed of Sound									
This work	181	DPPE	0.27–0.97	230–373	0.18–10.41	0.27	-0.15	0.28	-0.65
Ideal-Gas Heat Capacity									
This work	47	Sim	0.8–2.8	100–1000	0	0.68	0.39	0.63	1.34
Heat of Vaporization									
Raabe, 2020 [6]	7	Sim	0.2–2.8	278–353	0.10–1.21	2.99	2.87	5.88	17.21

[a]Number of available data points.
[b]VTD: vibrating tube densimeter; Sim: simulated data; PTx: pressure, temperature, composition in fixed volume cell; VLE: vapor-liquid equilibrium apparatus; DPPE: dual-path pulse-echo apparatus.
[c]Relative expanded uncertainty for property X; NA indicates values were not available.
[d]Temperature range of available data.
[e]Pressure range of available data.
[f]Average absolute relative deviation (%) calculated according to Eq. 2.
[g]Bias (%) calculated according to Eq. 22.
[h]Standard deviation (%) calculated according to Eq. 23.
[i]Maximum relative deviation (%) calculated according to Eq. 3.

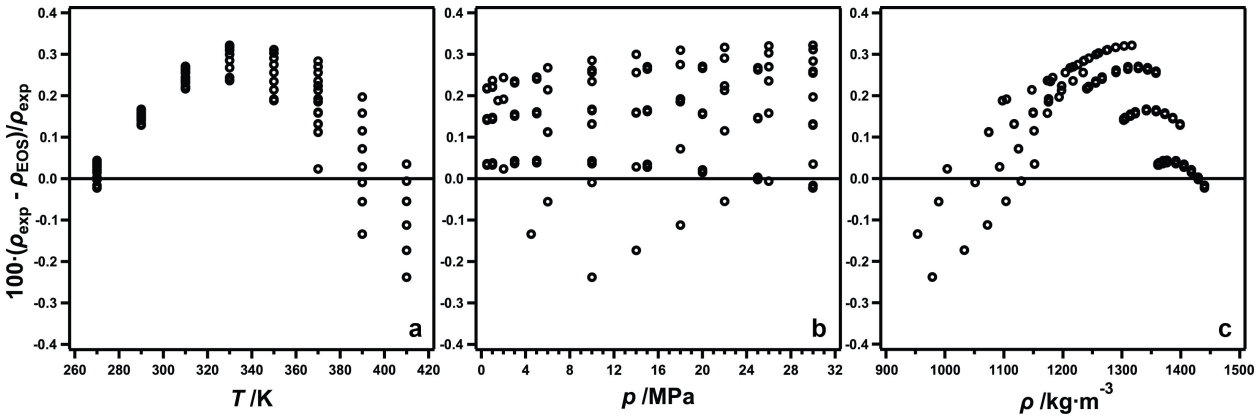

Fig. 8. Relative deviations of experimental density data for R-1336yf from values calculated with the new EOS, plotted as a function of (a) temperature, (b) pressure, and (c) density.

No experimental measurement results for saturated densities were found in the literature. Raabe [6] presented results from molecular simulations for both saturated liquid and saturated vapor densities. The simulation data were not used in the fitting process; they were used only for comparisons, the results of which are shown in Fig. 9. The saturated liquid data show good agreement with the EOS, with an AARD of 1.27 %. The saturated vapor data show much larger deviations, with an AARD of 12.16 % and a positive bias.

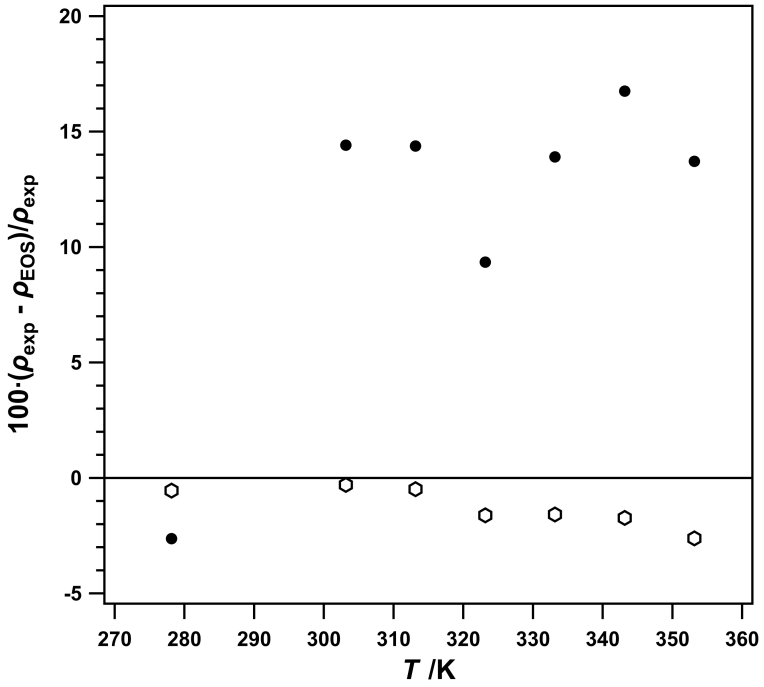

Fig. 9. Relative deviations of simulated saturated densities [6] for R-1336yf from values calculated with the new EOS, plotted as a function of temperature. Results are shown for saturated liquid (⬡) and saturated vapor (●).

There are two sources of experimental data for vapor pressure, and one set of data from molecular simulation [6]. The measurements in this work cover a temperature range of 265 K to 360 K and were the only vapor pressure measurements used in the regression. The other source of experimental data is from a patent [5] and are limited to 303 K and, as shown in Fig. 10, are in excellent agreement with our data. The molecular simulation values of Raabe [6] show deviations of approximately -2 % to 15 %. At a level of k = 2, the EOS represents the experimental vapor pressures from this work to within 3.06 %, with an AARD of 1.15 %. The highest deviation, 4.63 %, occurs at the lowest temperature where the vapor pressures are smallest; for this point the magnitude of the deviation is ~ 3 kPa.

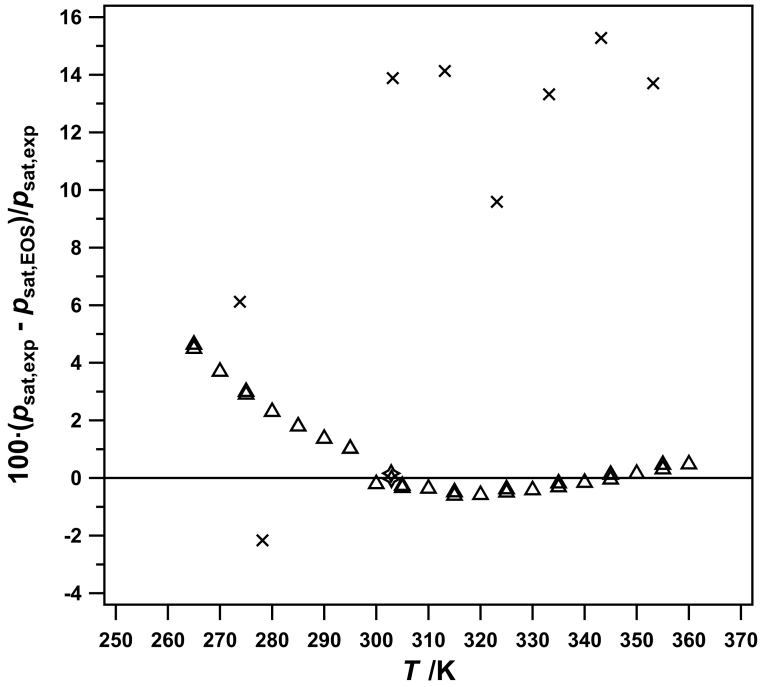

Fig. 10. Relative deviations of vapor pressure data for R-1336yf from values calculated with the new EOS, plotted as a function of temperature. Results are shown for the experimental data from this work (△) and from Robin and Kontomaris [5] (✧), and for the simulation data from Raabe [6] (✕).

The only source of speed of sound data are the measurements in this study, all of which are in the liquid phase, covering temperatures from 230 K to 373 K and pressures from 0.18 MPa to 10.41 MPa. Relative deviations of the liquid-phase speed of sound data from the EOS are shown in Figs. 11a and 11b, plotted as a function of temperature and pressure, respectively. At a level of k = 2, the data are represented to within 0.56 %, with an AARD of 0.27 %.

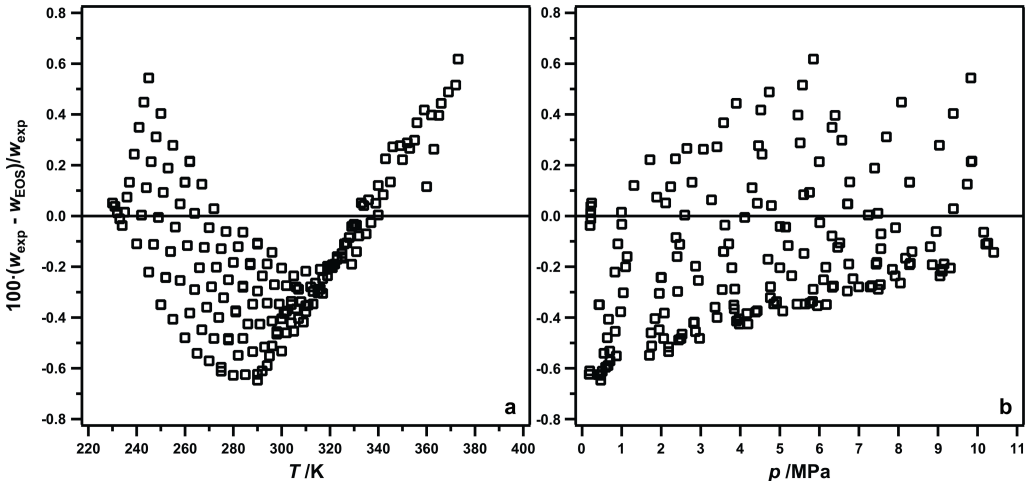

Fig. 11. Relative deviations of experimental speed of sound data for R-1336yf from values calculated with the new EOS, plotted as a function of (a) temperature and (b) pressure.

No experimental measurements were found for the heat of vaporization, but Raabe [6] presented data from molecular simulation for the temperature range 278 K to 353 K. They show good agreement with the EOS, except for the lowest temperature, with an AARD of 2.99 %. The relative deviations from the EOS are illustrated in Fig. 12.

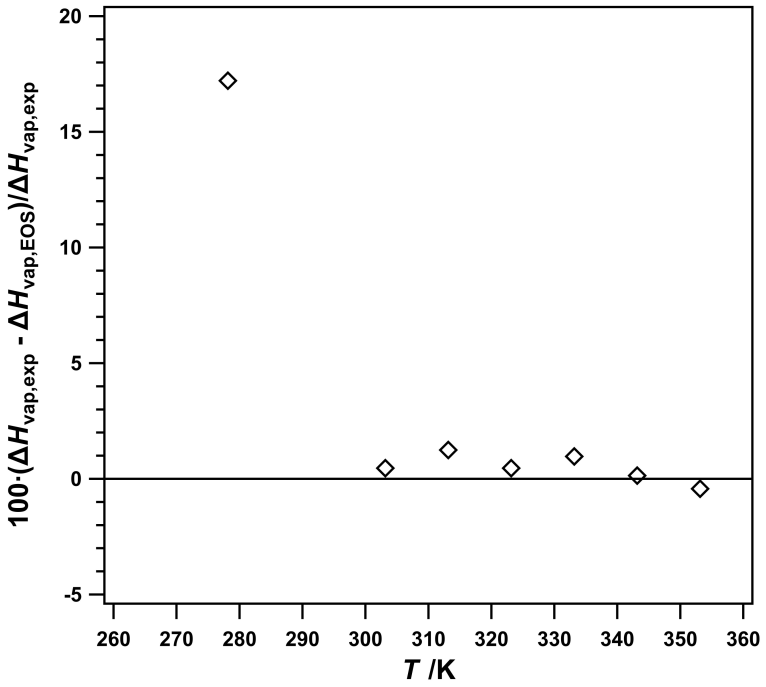

Fig. 12. Relative deviations of simulated heats of vaporization [6] for R-1336yf, plotted as a function of temperature.

4.3 Extrapolation Behavior

In this section we provide selected plots of derived properties from the equation of state to demonstrate the behavior in extrapolated regions where there are no experimental data. First, virial coefficients can be calculated from the equation of state with thermodynamic relationships as described in Lemmon and Jacobsen [23]. Thol et al. [44] observed some qualitative features of the behavior of calculated virial coefficients for the Lennard-Jones fluid. The second virial coefficient, B, approaches negative infinity at zero temperature, passes through zero at the Boyle temperature, goes through a maximum at the Joule-Thomson inversion temperature, and then approaches zero at extremely high temperatures. The third virial coefficient, C, also approaches negative infinity at zero temperature, passes through zero at a moderate temperature, reaches a maximum and then decreases as the temperature increases. The fourth virial coefficient, D, has similar behavior to C but for Lennard-Jones fluids has an additional maximum of a smaller magnitude at high temperatures. Fig. 13 demonstrates that the virial coefficients calculated from the EOS show this same behavior.

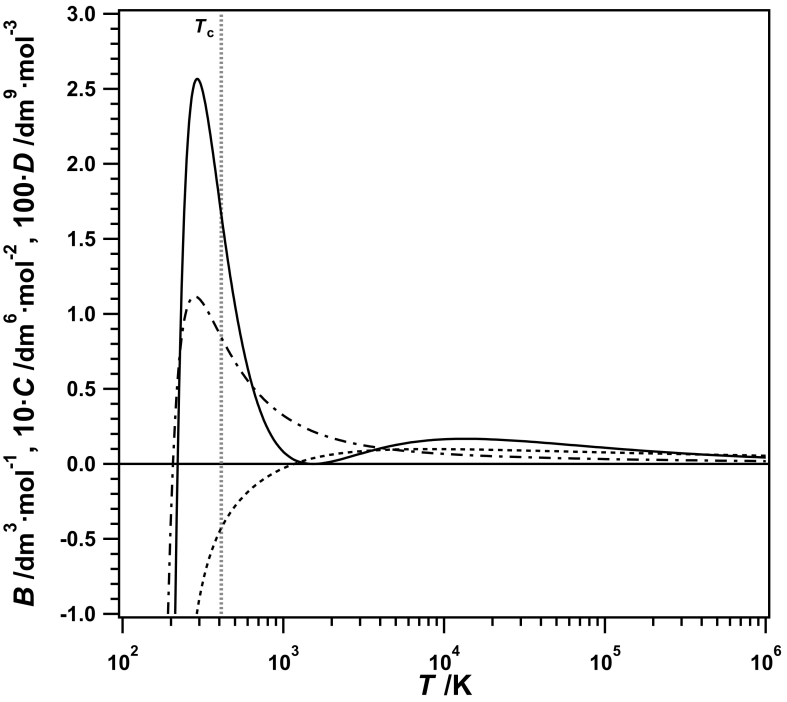

Fig. 13. Virial coefficients calculated with the new EOS as a function of temperature. Shown are the second virial (B, ----), the third virial (C, – · –), and the fourth virial (D, ——). Note that C and D are plotted as 10· C and 100· D, respectively. The gray dotted line (·····) marks the critical temperature (T_c).

Next, plots of ideal curves are useful in assessing the extrapolation behavior of an EOS in regions where data are unavailable [23, 45, 46]. Along an ideal curve, the property of a real fluid corresponds to a hypothetical ideal fluid at the same temperature and density. When applied to the compressibility factor Z, these are known as the Boyle curve,

$$\left(\frac{\partial Z}{\partial v}\right)_T = 0, \tag{24}$$

the Joule-Thomson inversion curve,

$$\left(\frac{\partial Z}{\partial T}\right)_p = 0, \tag{25}$$

the Joule inversion curve,

$$\left(\frac{\partial Z}{\partial T}\right)_v = 0, \tag{26}$$

and the ideal curve,

$$Z = \frac{p}{\rho RT} = 1. \tag{27}$$

These curves, along with the vapor pressure curve, are shown in Fig. 14. There is a very slight wiggle in the Joule inversion curve at very high temperatures and pressures, but other than that, there are no large bumps or unusual changes in slope, indicating that the extrapolation behavior to extreme conditions is qualitatively correct.

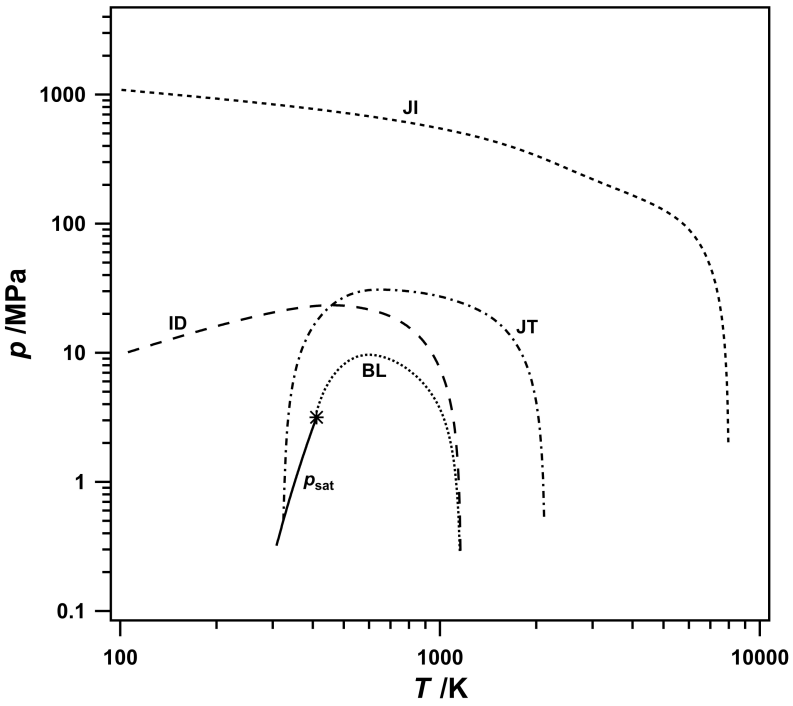

Fig. 14. Ideal curves to test extrapolation behavior, plotted as pressure vs temperature. Shown are the ideal curve (ID, – –) (Eq. 27), the Boyle curve (BL, ·····) (Eq. 24), the Joule-Thomson inversion curve (JT, – · –) (Eq. 25), and the Joule inversion curve (JI, - - - -) (Eq. 26). Also shown are the vapor pressure curve (p_{sat}, ——) and the critical point (✳).

Another test of the extrapolation behavior of an EOS involves examining the behavior along isotherms at extreme conditions. Figure 15 shows a pressure-density plot along isotherms at extreme conditions. There is no unusual behavior evident at temperatures up to 10^9 K and pressures of ~ 10^{14} MPa.

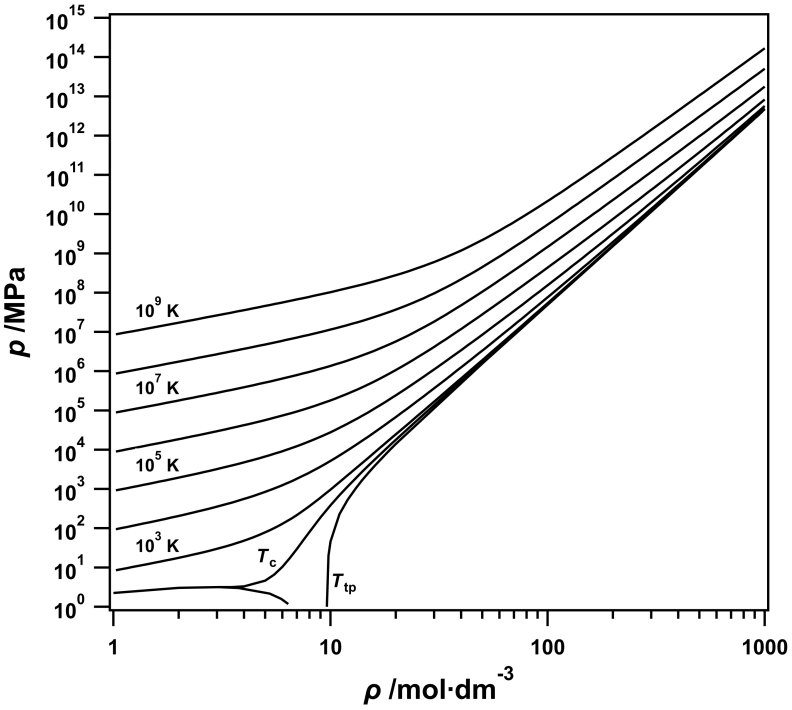

Fig. 15. Pressure versus density along isotherms at extreme conditions.

5. Conclusions

Thermophysical property measurement results for R-1336yf have been reported in this work. Density measurements covered temperatures from 270 K to 410 K and pressures from 0.5 MPa to 30 MPa and were conducted using an automated vibrating tube densimeter. At these temperatures and pressures, the sample remained in the compressed liquid phase throughout, and the measured densities ranged from approximately 954 $kg \cdot m^{-3}$ to 1440 $kg \cdot m^{-3}$. Vapor pressure measurements covered temperatures from 265 K to 360 K and were conducted using a vapor-liquid equilibrium apparatus; measured values ranged from approximately 68 kPa to 1220 kPa. Speed of sound measurements covered temperatures from 230 K to 373 K and pressures up to 10 MPa and were conducted using a dual-path pulse-echo apparatus. Measured liquid sound speeds ranged from approximately 290 $m \cdot s^{-1}$ to 771 $m \cdot s^{-1}$. These experimental data, along with computational chemistry calculations for the ideal-gas heat capacity, were used to develop a preliminary Helmholtz equation of state for this fluid. The equation was validated against our experimental measurements from 230 K to 410 K at pressures up to 30 MPa. The relative combined expanded (k = 2) uncertainty estimates over the validated range of conditions are 0.24 % for liquid density, 0.56 % for liquid-phase speed of sound, 3.06 % (or within ~ 3 kPa) for vapor pressure, and 1 % - 3 % for ideal-gas heat capacity (or ~ 2 $J \cdot mol^{-1} \cdot K^{-1}$). Testing indicated that the EOS exhibits qualitatively correct extrapolation behavior, and we recommend it for use from the estimated triple-point temperature of 195 K, up to slightly above the critical temperature of 425 K, and for pressures up to 30 MPa. Although the uncertainties may be higher for temperatures below 230 K and above 410 K, we feel that the EOS can be safely used over this range of conditions for engineering calculations.

References

[1] Bell IH, Domanski PA, McLinden MO, Linteris GT (2019) The Hunt for Nonflammable Refrigerant Blends to Replace R-134a. *Int J Refrig* 104:484-495.
[2] Domanski PA, Brignoli R, Brown JS, Kazakov AF, McLinden MO (2017) Low-GWP Refrigerants for Medium and High-Pressure Applications. *Int J Refrig* 84:198-209.
[3] McLinden MO, Brown JS, Brignoli R, Kazakov AF, Domanski PA (2017) Limited Options for Low-Global-Warming-Potential Refrigerants. *Nat Commun* 8:14476.
[4] McLinden MO, Kazakov AF, Brown JS, Domanski PA (2014) A Thermodynamic Analysis of Refrigerants: Possibilities and Tradeoffs for Low-GWP Refrigerants. *Int J Refrig* 38:80-92.
[5] Robin ML , Kontomaris K (2013) Azeotropic and Azeotropic-Like Compositions of 2,3,3,4,4,4-Hexafluoro-1-butene and 1,1,1,2,3,3-Hexafluoropropane and Its Uses Thereof. WO 2014/028697.
[6] Raabe G (2020) Purely Predictive Vapor–Liquid Equilibrium Properties of 3,3,4,4,4-Pentafluoro-1-butene (HFO-1345fz), 2,3,3,4,4,4-Hexafluoro-1-butene (HFO-1336yf), and *trans*-1-Chloro-2,3,3,3-tetrafluoropropene (HCFO-1224yd(E)) from Molecular Simulation. *J Chem Eng Data* 65(9):4318-4325.
[7] Hanwell MD, Curtis DE, Lonie DC, Vandermeersch T, Zurek E, Hutchison GR (2012) Avogadro: An Advanced Semantic Chemical Editor, Visualization, and Analysis Platform. *J Cheminform* 4:17.
[8] Outcalt SL , McLinden MO (2007) Automated Densimeter for the Rapid Characterization of Industrial Fluids. *Ind Eng Chem Res* 46:8264-8269.
[9] Outcalt SL , Rowane AJ (2021) Bubble Point Measurements of Mixtures of HFO and HFC Refrigerants. *J Chem Eng Data* 66:4670-4683.
[10] McLinden MO , Perkins RA (2023) A Dual-Path Pulse-Echo Instrument for Liquid-Phase Speed of Sound and Measurements on *p*-Xylene and Four Halogenated-Olefin Refrigerants [R1234yf, R1234ze(E), R1233zd(E), and R1336mzz(Z)]. *Ind Eng Chem Res* 62:12381-12406.
[11] Rowane AJ , Perkins RA (2022) Speed of Sound Measurements of Binary Mixtures of 1,1,1,2-Tetrafluoroethane (R-134a), 2,3,3,3-Tetrafluoropropene (R-1234yf), and *trans*-1,3,3,3-Tetrafluoropropene (R-1234ze(E)) Refrigerants. *J Chem Eng Data* 67:1365-1377.
[12] Outcalt SL (2018) Calibration Fluids and Calibration Equations: How Choices May Affect the Results of Density Measurements Made with U-Tube Densimeters. *J Res Natl Inst Stand Technol* 123:123017.
[13] May EF, Tay WJ, Nania M, Aleji A, Al-Ghafri S, Trusler JPM (2014) Physical Apparatus Parameters and Model for Vibrating Tube Densimeters at Pressures to 140 MPa and Temperatures to 473 K. *Rev Sci Instrum* 85:095111.
[14] McLinden MO , Akasaka R (2020) Thermodynamic Properties of *cis*-1,1,1,4,4,4-Hexafluorobutene [R-1336mzz(Z)]: Vapor Pressure, (p, ρ, T) Behavior, and Speed of Sound Measurements and Equation of State. *J Chem Eng Data* 65:4201-4214.
[15] Lemmon EW, Bell IH, Huber ML, McLinden MO (2018) NIST Standard Reference Database 23: Reference Fluid Thermodynamic and Transport Properties (REFPROP) (National Institute of Standards and Technology, Gaithersburg, MD), 10.0. http://www.nist.gov/srd/nist23.cfm
[16] Trusler JPM (1991) *Physical Acoustics and Metrology of Fluids* (CRC Press, Boca Raton, FL).

[17] Lemmon EW, McLinden MO, Wagner W (2009) Thermodynamic Properties of Propane. III. A Reference Equation of State for Temperatures from the Melting Line to 650 K and Pressures up to 1000 MPa. *J Chem Eng Data* 54(12):3141-3180.
[18] Rowane AJ , Rasmussen EG (2025) Speed of Sound Measurements of Binary Mixtures of *trans*-1,2-Difluoroethylene (R-1132(E)) with Difluoromethane (R-32) or 2,3,3,3-Tetrafluoropropene (R-1234yf). *J Chem Eng Data* 70:817-826.
[19] Fortin TJ , Outcalt SL (2025) Compressed Liquid (p-ρ-T) Measurements of *trans*-1,2-Dichloroethene [R1130(E)]. *Int J Thermophys* 46:74.
[20] International Organization for Standardization (ISO) (1995) Guide to the Expression of Uncertainty in Measurement. (ISO, Geneva, Switzerland).
[21] Rowane AJ , Outcalt SL (2024) Bubble Point Measurements of *cis*-1,1,1,4,4,4-Hexafluorobutene [R-1336mzz(Z)] + *trans*-1,2-Dichloroethene [R1130(E)] Mixtures. *Int J Thermophys* 45:96.
[22] Pan J, Rui X, Zhao X, Qiu L (2012) An Equation of State for the Thermodynamic Properties of 1,1,1,3,3,3-Hexafluoropropane (HFC-236fa). *Fluid Phase Equilib* 321:10-16.
[23] Lemmon EW , Jacobsen RT (2005) A New Functional Form and New Fitting Techniques for Equations of State with Application to Pentafluoroethane (HFC-125). *J Phys Chem Ref Data* 34(1):69-108.
[24] Mohr PJ, Newell DB, Taylor BN, Tiesinga E (2025) CODATA Recommended Values of the Fundamental Physical Constants: 2022. *J Phys Chem Ref Data* 54:033105.
[25] Wieser ME , Berglund M (2009) Atomic Weights of the Elements 2007 (IUPAC Technical Report). *Pure Appl Chem* 81(11):2131-2156.
[26] Design Institute for Physical Properties (DIPPR) (2023) DIPPR Project 801 Database (Brigham Young University, Provo, Utah), Sponsor Version.
[27] Grimme S, Ehrlich S, Goerigk L (2011) Effect of the Damping Function in Dispersion Corrected Density Functional Theory. *J Comput Chem* 32(7):1456-1465.
[28] Weigend F , Ahlrichs R (2005) Balanced Basis Sets of Split Valence, Triple Zeta Valence and Quadruple Zeta Valence Quality for H to Rn: Design and Assessment of Accuracy. *Phys Chem Chem Phys* 7(18):3297-3305.
[29] Santra G, Sylvetsky N, Martin JML (2019) Minimally Empirical Double-Hybrid Functionals Trained Against the GMTKN55 Database: revDSD-PBEP86-D4, revDOD-PBE-D4, and DOD-SCAN-D4. *J Phys Chem A* 123(24):5129-5143.
[30] Rappoport D , Furche F (2010) Property-Optimized Gaussian Basis Sets for Molecular Response Calculations. *J Chem Phys* 133(13):134105.
[31] Paulechka E , Kazakov A (2017) Efficient DLPNO-CCSD(T)-Based Estimation of Formation Enthalpies for C-, H-, O-, and N-Containing Closed-Shell Compounds Validated Against Critically Evaluated Experimental Data. *J Phys Chem A* 121(22):4379-4387.
[32] Nagy PR, Samu G, Kállay M (2016) An Integral-Direct Linear-Scaling Second-Order Møller–Plesset Approach. *J Chem Theory Comput* 12(10):4897-4914.
[33] Nagy PR , Kállay M (2017) Optimization of the Linear-Scaling Local Natural Orbital CCSD(T) Method: Redundancy-Free Triples Correction Using Laplace Transform. *J Chem Phys* 146(21):214106.
[34] Kendall RA, Dunning TH, Jr., Harrison RJ (1992) Electron Affinities of the First-Row Atoms Revisited. Systematic Basis Sets and Wave Functions. *J Chem Phys* 96(9):6796-6806.

[35] Frisch MJ, Trucks GW, Schlegel HB, Scuseria GE, Robb MA, Cheeseman JR, Scalmani G, Barone V, Petersson GA, Nakatsuji H, Li X, Caricato M, Marenich AV, Bloino J, Janesko BG, Gomperts R, Mennucci B, Hratchian HP, Ortiz JV, Izmaylov AF, Sonnenberg JL, Williams, Ding F, Lipparini F, Egidi F, Goings J, Peng B, Petrone A, Henderson T, Ranasinghe D, Zakrzewski VG, Gao J, Rega N, Zheng G, Liang W, Hada M, Ehara M, Toyota K, Fukuda R, Hasegawa J, Ishida M, Nakajima T, Honda Y, Kitao O, Nakai H, Vreven T, Throssell K, Montgomery Jr. JA, Peralta JE, Ogliaro F, Bearpark MJ, Heyd JJ, Brothers EN, Kudin KN, Staroverov VN, Keith TA, Kobayashi R, Normand J, Raghavachari K, Rendell AP, Burant JC, Iyengar SS, Tomasi J, Cossi M, Millam JM, Klene M, Adamo C, Cammi R, Ochterski JW, Martin RL, Morokuma K, Farkas O, Foresman JB, Fox DJ (2016) Gaussian 16, Rev. C.01 (Gaussian, Inc., Wallingford, CT)

[36] Kállay M, Nagy PR, Mester D, Rolik Z, Samu G, Csontos J, Csóka J, Szabó PB, Gyevi-Nagy L, Hégely B, Ladjánszki I, Szegedy L, Ladóczki B, Petrov K, Farkas M, Mezei PD, Ganyecz Á (2020) The MRCC Program System: Accurate Quantum Chemistry from Water to Proteins. *J Chem Phys* 152(7):074107.

[37] Diky V, Chirico RD, Frenkel M, Bazyleva A, Magee JW, Paulechka E, Kazakov A, Lemmon EW, Muzny CD, Smolyanitsky AY, Townsend S, Kroenlein K (2019) NIST Standard Database 103b: ThermoData Engine (TDE) (National Institute of Standards and Technology, Gaithersburg, MD), 10.4. https://www.nist.gov/mml/acmd/trc/thermodata-engine/srd-nist-tde-103b

[38] Elliott JR, Diky V, Knotts TA, Wilding WV, eds (2023) *The Properties of Gases and Liquids* (McGraw Hill, New York, NY), 6th Ed.

[39] Akasaka R , Lemmon EW (2025) A Helmholtz Energy Equation of State for 3,3,3-Trifluoroprop-1-ene (R-1243zf). *Int J Thermophys* 46:23.

[40] Huber ML, Kazakov AF, Lemmon EW (2025) Equation of State for the Thermodynamic Properties of *trans*-1,2-Dichloroethene [R-1130(E)]. *Int J Thermophys* 46:76.

[41] Akasaka R , Lemmon EW (2019) Fundamental Equations of State for *cis*-1,3,3,3-Tetrafluoropropene [R-1234ze(Z)] and 3,3,3-Trifluoropropene (R-1243zf). *J Chem Eng Data* 64(11):4679-4691.

[42] Akasaka R , Lemmon EW (2024) A Helmholtz Energy Equation of State for Calculations of Thermodynamic Properties of *trans*-1,2-Difluoroethene [R-1132(E)]. *Int J Thermophys* 45.

[43] Wagner W (1972) A Method to Establish Equations of State Exactly Representing all Saturated State Variables Applied to Nitrogen. *Cryogenics* 12(3):214-221.

[44] Thol M, Rutkai G, Span R, Vrabec J, Lustig R (2015) Equation of State for the Lennard-Jones Truncated and Shifted Model Fluid. *Int J Thermophys* 36(1):25-43.

[45] Span R (2000) *Multiparameter Equations of State - An Accurate Source of Thermodynamic Property Data* (Springer, Berlin, Germany).

[46] Span R , Wagner W (1997) On the Extrapolation Behavior of Empirical Equations of State. *Int J Thermophys* 18(6):1415-1443.

[47] Huber ML (2018) Models for the Viscosity, Thermal Conductivity, and Surface Tension of Selected Pure Fluids as Implemented in REFPROP v10.0. (National Institute of Standards and Technology, Gaithersburg, MD), NISTIR 8209.

[48] Akasaka R, Huber ML, Simoni LD, Lemmon EW (2023) A Helmholtz Energy Equation of State for *trans*-1,1,1,4,4,4-Hexafluoro-2-butene [R-1336mzz(E)] and an Auxiliary Extended Corresponding States Model for the Transport Properties. *Int J Thermophys* 44(4):50.

[49] Chung TH, Ajlan M, Lee LL, Starling KE (1988) Generalized Multiparameter Correlation for Nonpolar and Polar Fluid Transport Properties. *Ind Eng Chem Res* 27(4):671-679.

Supporting Information

A.1. Experimental Data

The experimental density, vapor pressure, and speed of sound data presented in Tables 2–4 are available for download as tab-delimited text files at https://doi.org/10.18434/mds2-3644.

A.2. Modeling

The equation of state developed in this work is available for download as a REFPROP fluid file (R1336YF.FLD) at https://doi.org/10.18434/mds2-3644. Additional information regarding the transport property modeling, as well as sample Python code, are included in the following sections.

A.2.1. Transport Property Modeling

No experimental data are available in the literature for the viscosity or the thermal conductivity of R-1336yf. Since many engineering applications require these properties, we developed a predictive model that can be used to provide estimates for viscosity and thermal conductivity. We used an extended corresponding states (ECS) model described in Huber [47] that is currently implemented in REFPROP [15]. Due to the lack of data, we use the model recently developed for R-1336mzz(E) [48] as an estimate. R-1336mzz(E), or *trans*-1,1,1,4,4,4-hexafluoro-2-butene ($C_4H_2F_6$), is an isomer of R-1336yf. There is another isomer, R-1336mzz(Z), (Z)-1,1,1,4,4,4-hexafluoro-2-butene ($C_4H_2F_6$), for which we have a transport model, but the vapor pressure curve of R-1336yf is much closer to R-1336ze(E) than it is to R-1336mzz(Z) so we chose the R-1336zz(E) isomer. Since the critical point of R-1336yf is different than R-1336mzz(E), we needed to recompute the Lennard-Jones parameters using the method of Chung et al. [49] together with the critical temperature (T_c), critical density (ρ_c), and acentric factor (ω) values for R-1336yf that were determined in this work, namely 411.02 K, 3167.06 kPa, and 0.2885. We obtained σ = 0.5578 nm and ε/k_B = 326.39 K where σ is the Lennard-Jones collision diameter, ε is the Lennard-Jones potential energy, and k_B is the Boltzmann constant. We also adjusted the value of F_c in the Chung et al. [49] model, which corrects for molecular structure and polar effects, from 0.7619 for R-1336mzz(E) to 0.8109 for R-1336yf due to differences in their dipole moments and critical points. We retained all other ECS parameters from the model for R-1336mzz(E) [48] and these are implemented in the R1336YF.FLD file which is available for download at https://doi.org/10.18434/mds2-3644. It is difficult to assess the uncertainty due to the lack of data, but based on previous work on similar refrigerants we estimate the uncertainty in both viscosity and thermal conductivity to be 15 %.

A.2.2. Sample Python Code

Sample Python code that can be used to reproduce the values found in Table 10 of the manuscript is shown below.

```
# Test code to implement a Helmholtz EOS for R1336YF

# Import necessary functions from the math library
from math import exp, log, sqrt

# Define constants for R1336YF
Tc = 411.02             # Critical temperature (K)
rhoc = 3050.0           # Critical density (mol/m^3)
a1 = -14.75787030085678
a2 = 10.2338799972408516
c0 = 4
u = [318, 1137, 3221]     # Constants for ideal gas terms
v = [9.529, 14.083, 6.385]
Npoly = 6
Nexp = 5
NGauss = 4
M = 164.0490992 / 1000.0  # Molar mass (kg/mol)
R = 8.314462618         # Molar gas constant (J/mol/K)

# Coefficients for the equation of state
n = [0.0293023,0.54634,0.051,0.146,-0.1140088219803,-0.9899987857495,-0.383,-0.83,-0.091,-0.01078,-
0.03861,-0.224,-0.04161,-0.24598,-0.1595]
t = [1.0,0.154,0.2275,0.455,0.75,1.176,1.14,1.34,6.3,6.5,4.9,1.6,1.5,1.4,1.45]
d = [4, 1, 2, 3, 1, 2, 1, 1, 1, 2, 3, 1, 2, 1, 1]
l = [0, 0, 0, 0, 0, 0, 1, 2, 3, 3, 3] + [0] * 4
g = [0, 0, 0, 0, 0, 0, 2.55, 0.996, 0.719, 2.7955, 0.294] + [0] * 4
eta = [0] * 11 + [2.34, 1.216, 4.115, 1.391]
beta = [0] * 11 + [0] * 4
gamma = [0] * 11 + [1] * 4
epsilon = [0] * 11 + [-0.075, 1.12, -0.328, 0.912]

# Function to calculate residual derivatives
def resid_derivs(T, rho):
    tau = Tc / T        # Reduced temperature
    delta = rho / rhoc   # Reduced density

    # Initialize derivatives
    A00 = A10 = A01 = A20 = A11 = A02 = 0

    # Polynomial terms
    for i in range(Npoly):
        term = n[i] * delta**d[i] * tau**t[i]
        A00 += term
        A10 += t[i] * term
        A01 += d[i] * term
        A20 += t[i] * (t[i] - 1) * term
        A11 += d[i] * t[i] * term
        A02 += d[i] * (d[i] - 1) * term

    # Exponential terms
    for i in range(Npoly, Npoly + Nexp):
        exp_term = exp(-g[i] * delta**l[i])
        term = n[i] * delta**d[i] * tau**t[i] * exp_term
        A00 += term
        A10 += t[i] * term
```

```
        A01 += term * (d[i] - l[i] * g[i] * delta**l[i])
        A20 += t[i] * (t[i] - 1) * term
        A11 += t[i] * term * (d[i] - l[i] * g[i] * delta**l[i])
        A02 += term * ((d[i] - l[i] * g[i] * delta**l[i]) * (d[i] - 1 - l[i] * g[i] * delta**l[i]) - l[i]**2 * g[i] * delta**l[i])

    # Gaussian terms
    for i in range(Npoly + Nexp, Npoly + Nexp + NGauss):
        exp_term = exp(-eta[i] * (delta - epsilon[i])**2 - beta[i] * (tau - gamma[i])**2)
        term = n[i] * delta**d[i] * tau**t[i] * exp_term
        A00 += term
        A10 += term * (t[i] - 2 * beta[i] * tau * (tau - gamma[i]))
        A01 += term * (d[i] - 2 * eta[i] * delta * (delta - epsilon[i]))
        A20 += term * ((t[i] - 2 * beta[i] * tau * (tau - gamma[i]))**2 - t[i] - 2 * beta[i] * tau**2)
        A11 += term * (t[i] - 2 * beta[i] * tau * (tau - gamma[i])) * (d[i] - 2 * eta[i] * delta * (delta - epsilon[i]))
        A02 += term * ((d[i] - 2 * eta[i] * delta * (delta - epsilon[i]))**2 - d[i] - 2 * eta[i] * delta**2)

    return A00, A10, A01, A20, A11, A02

# Ideal Derivatives Function
def ideal_derivs(T, rho):
    tau = Tc / T
    delta = rho / rhoc
    A01 = 1
    A02 = -1
    A11 = 0
    A00 = log(delta) if delta > 0 else 0
    A00 += a1 + a2 * tau + (c0 - 1) * log(tau)
    for i in range(len(u)):
        A00 += v[i] * log(1 - exp(-u[i] * tau / Tc))
    A10 = a2 * tau + (c0 - 1)
    for i in range(len(u)):
        A10 += tau * v[i] * (u[i] / Tc) / (exp(u[i] * tau / Tc) - 1)
    A20 = -(c0 - 1)
    for i in range(len(u)):
        A20 -= tau**2 * v[i] * (u[i] / Tc)**2 * exp(u[i] * tau / Tc) / (exp(u[i] * tau / Tc) - 1)**2
    return A00, A10, A01, A20, A11, A02

# Function to combine residual and ideal derivatives
def derivs(T, rho):
    resid = resid_derivs(T, rho)
    ideal = ideal_derivs(T, rho)

    # Add corresponding terms from residual and ideal derivatives
    combined = [resid[i] + ideal[i] for i in range(len(resid))]
    return combined

# Main function to calculate and display thermodynamic properties
def main():
    # Temperature (T in K) and density (rho in mol/L) values to test
    test_cases = [
        (300, 0.),
        (300, 0.01),
        (300, 8.0),
        (400, 6.0),
        (400, 0.2),
```

```
    (420,5.0)
  ]

  # Print table header
  print(f"{'T (K)':<10}{'rho (mol/L)':<15}{'p (MPa)':<10}{'w (m/s)':<10}{'cp (J/mol/K)':<15}{'cv
(J/mol/K)':<15}{'h (J/mol)':<15}")
  print("-" * 83)

  for T, rho in test_cases:
    rho = rho * 1000              # Convert density to mol/m^3
    Ar00, Ar10, Ar01, Ar20, Ar11, Ar02 = resid_derivs(T, rho)
    A00, A10, A01, A20, A11, A02 = derivs(T, rho)

    # Calculate pressure (p), speed of sound (w), heat capacities (cp, cv), and enthalpy (h)
    p = rho * R * T * (Ar01 + 1) / 1e6  # Pressure in MPa
    cv = -R * A20
    cp = cv + R * (1 + Ar01 - Ar11)**2 / (1 + 2 * Ar01 + Ar02)
    w = sqrt(R * T / M * ((1 + 2 * Ar01 + Ar02) - (1 + Ar01 - Ar11)**2 / A20))
    h = R * T * (A10 + Ar01 + 1)
    # Print the results as a table row
    print(f"{T:<10}{rho / 1000:<15.2f}{p:<10.5f}{w:<10.3f}{cp:<15.3f}{cv:<15.3f}{h:<15.1f}")

# Run the main function if this script is executed
if __name__ == '__main__':
  main()
```